

FishBack: Pullback Fisher Geometry for Optimal Activation Steering in Transformers

Sihan Wang,¹ Jiayi Zhao¹

¹South China University of Technology
cswangsihan@mail.scut.edu.cn

Abstract

Activation steering methods modify intermediate representations of language models to control output behavior, but universally assume the activation space is Euclidean. We show this assumption fails drastically: the local geometry induced by the model’s own output behavior—the Fisher information metric of the softmax layer, pulled back through the Jacobian of subsequent layers—deviates from the Euclidean metric by over 97% in relative spectral norm on GPT-2, with an effective dimensionality of only 2–17% of the ambient space. From this pullback Fisher metric, we derive a closed-form steering equation that identifies the minimum-distortion direction for any target concept, yielding a closed-form optimal direction at each point that can be applied iteratively without manifold fitting or data-driven geometry estimation. We call the resulting framework **FishBack**. The metric admits a layer-wise recursive decomposition, which reveals that existing methods—CAA, ActAdd, ITI, and others—each implicitly adopt a particular approximate metric, and that their performance gaps are quantitatively predicted by a single spectral diagnostic: the ratio of their implicit metric’s cost to the Fisher-optimal cost. On GPT-2, iterative pullback steering consistently outperforms all Euclidean baselines across three verb-morphology concepts and four layers, with off-target KL reductions of **1.3x–2.5x** relative to Euclidean gradient ascent and **1.5x** relative to CAA at matched concept probability.

1 Introduction

Activation steering—directly modifying the intermediate representations of a language model at inference time to alter its output behavior—has become a central technique for model interpretability and control (Turner et al. 2024; Rimsky et al. 2024; Zou et al. 2023; Li et al. 2023). By adding a carefully chosen direction vector to a hidden state, practitioners can shift model outputs toward desired concepts such as truthfulness (Li et al. 2023), sentiment (Turner et al. 2024), or safety compliance (Arditi et al. 2024), without retraining. Yet in practice, these methods are notably fragile. The effectiveness of a steering vector varies dramatically across layers, with interventions that succeed at one depth failing or degrading output quality at another (Turner et al. 2024; van der Weij, Poesio, and Schoots 2024). The scaling coefficient must be tuned within a narrow viable range: too small and the effect vanishes; too large and the model degenerates into repetition or incoherent text (Vu and Nguyen

2025). These failure modes have been documented across architectures, tasks, and model scales (van der Weij, Poesio, and Schoots 2024; Vu and Nguyen 2025), but their root cause has remained unclear. In this work, we trace them to a shared source: every existing steering method implicitly assumes that the intermediate activation space is Euclidean—that all directions are equally costly to perturb, and that the natural way to modify a representation is vector addition. We show that this assumption is not merely approximate but fundamentally wrong.

Prior work on activation steering can be organized along two axes: *where* the geometry is defined and *how* it is obtained. The largest family of methods operates in intermediate layers under the Euclidean assumption, differing only in the strategy for selecting the steering direction: mean difference over contrastive pairs (Rimsky et al. 2024; Turner et al. 2024), linear probes on attention heads (Li et al. 2023), covariance-weighted projections (Singh et al. 2024), trained rank-one interventions (Wu et al. 2025), or concept erasure via optimal affine subspaces (Belrose et al. 2023). All of these execute the same additive update $h' = h + \alpha v$ and inherit its implicit Euclidean geometry. In a separate line of work, Park et al. (2026) rigorously establish that the natural geometry of the softmax output layer is the Fisher-Rao geometry induced by the KL divergence (Rao 1945; Amari 1998, 2016), and prove that steering along dual coordinates optimally preserves off-target semantics. Their theory, however, applies only to the final representation layer. More recently, Wurgaft et al. (2026) and Raval et al. (2026) empirically demonstrate that intermediate activation spaces exhibit significant geometric distortion and propose data-driven remedies based on manifold fitting or kernel PCA. While correctly identifying the problem, these approaches provide no formal characterization of the intermediate-layer geometry, no optimality guarantees for the resulting steering directions, and no explanation of why Euclidean methods sometimes work well despite using the wrong geometry.

Our key observation is that the correct intermediate-layer geometry need not be estimated from data—it can be *derived* from the model’s own computational structure. The output-layer Fisher information metric, which governs the softmax layer (Park et al. 2026; Banerjee et al. 2005), propagates backward through the Jacobian of each subsequent Transformer layer via the standard differential-geometric pullback

operation (Arvanitidis, Hansen, and Hauberg 2018; Arvanitidis et al. 2022). The resulting *pullback Fisher metric* is a closed-form, layer-specific, input-dependent Riemannian metric on the intermediate activation space that measures precisely how much each direction of perturbation affects the output distribution. On GPT-2, this metric deviates from the Euclidean metric by over 97% in relative spectral norm, with an effective dimensionality of only 2–17% of the ambient space—meaning that the vast majority of directions have negligible influence on model output, yet Euclidean steering treats them all equally. This extreme anisotropy is not an accident: the metric admits a layer-wise recursive decomposition through the residual blocks, whose structure—particularly the rank deficiency introduced by LayerNorm (Ba, Kiros, and Hinton 2016)—causes the condition number to grow with depth, providing a formal explanation for the layer sensitivity empirically observed across prior work. Crucially, this geometric framework also reveals that all existing steering methods implicitly operate under different approximate metrics, and that their empirical performance gaps can be quantitatively predicted by a unified spectral diagnostic rooted in the Fisher–Pythagorean decomposition of excess KL cost (Martens 2020).

Our main contributions are as follows:

- We derive the pullback Fisher metric for Transformer intermediate layers—analytically pulling back the output-layer Fisher information (Amari 2016) through the Jacobian of subsequent layers—and prove a closed-form optimal steering equation that yields the minimum off-target KL direction for any target concept via a single matrix solve. The equation can be applied iteratively with updated covectors and Fisher matrices, without manifold fitting or data-driven geometry estimation.
- We establish a unified information-geometric framework in which CAA, ActAdd, ITI, ReFT-r1, Representation Surgery, and Park’s dual steering are all instances of steering under specific implicit metrics. A Fisher–Pythagorean decomposition of the excess cost quantitatively predicts each method’s performance from a single spectral quantity, explaining both their successes and failures.
- We validate these theoretical predictions on GPT-2 with extensive experiments. The pullback Fisher metric exhibits condition numbers exceeding 10^7 and effective rank below 17%, confirming the failure of the Euclidean assumption. Iterative Fisher steering consistently outperforms all Euclidean baselines across three verb-morphology concepts and four layers. At matched concept probability, it reduces off-target KL by a median of $1.5\times$ relative to the strongest per-case baseline, with a win rate of 72% ($P < 10^{-4}$, binomial test).

2 Preliminaries

Transformer and intermediate-layer maps. We consider a decoder-only Transformer with L layers and hidden dimension d . Let $h^{(\ell)} \in \mathbb{R}^d$ denote the residual stream activation at the output of the ℓ -th layer for a given token position. Each layer applies a residual block $h^{(\ell+1)} = h^{(\ell)} +$

$F_\ell(h^{(\ell)})$, where F_ℓ comprises multi-head self-attention and a feedforward network, optionally preceded by layer normalization (Ba, Kiros, and Hinton 2016). Given a fixed input context, we define the *subsequent-layer map*

$$f^{(\ell)} : \mathbb{R}^d \rightarrow \mathbb{R}^d, \quad \lambda = f^{(\ell)}(h), \quad (1)$$

which maps a layer- ℓ activation h to the final hidden state λ produced after all remaining layers and the final layer normalization. Its Jacobian is $J = Df^{(\ell)}(h) \in \mathbb{R}^{d \times d}$. By the chain rule, $J = A_{L-1}A_{L-2} \cdots A_\ell$, where $A_k = I + DF_k(h^{(k)})$ is the Jacobian of the k -th residual block.

Softmax output distribution. The model produces a distribution over a vocabulary \mathcal{Y} with $|\mathcal{Y}|$ tokens via a linear unembedding layer followed by softmax. Each token $y \in \mathcal{Y}$ is associated with an unembedding vector $\gamma_y \in \mathbb{R}^d$ (a row of the weight matrix $W_U \in \mathbb{R}^{|\mathcal{Y}| \times d}$). Given a final hidden state $\lambda \in \mathbb{R}^d$, the output distribution is

$$P_\lambda(y) = \exp(\gamma_y^\top \lambda - A(\lambda)), \quad (2)$$

where $A(\lambda) = \log \sum_{y \in \mathcal{Y}} \exp(\gamma_y^\top \lambda)$ is the log-partition function. This is a $|\mathcal{Y}|$ -outcome categorical distribution in exponential family form with natural parameter λ and sufficient statistic γ_y .

The log-partition function A is strictly convex and infinitely differentiable. Its first and second derivatives yield two fundamental objects. The *dual coordinate* (or mean parameter) is $\phi(\lambda) = \nabla A(\lambda) = \mathbb{E}_{P_\lambda}[\gamma] = \sum_y P_\lambda(y) \gamma_y$, and the *Fisher information matrix* (equivalently, the Hessian of A) is

$$H(\lambda) = \nabla^2 A(\lambda) = \text{Cov}_{P_\lambda}(\gamma), \quad (3)$$

i.e., the covariance of the unembedding vectors under the current output distribution. The triple identity $\nabla^2 A = \text{Fisher} = \text{Cov}(\gamma)$ is standard for exponential families (Amari 2016; Banerjee et al. 2005).

KL divergence as Bregman divergence. The KL divergence between two output distributions admits a closed-form Bregman expression:

$$D_{\text{KL}}(P_{\lambda_0} \| P_{\lambda_1}) = A(\lambda_1) - A(\lambda_0) - \nabla A(\lambda_0)^\top (\lambda_1 - \lambda_0). \quad (4)$$

This identity, which follows directly from the exponential family form (2), makes explicit that the “distance” between representations is governed by the convex structure of A , not by the Euclidean norm $\|\lambda_1 - \lambda_0\|^2$. In particular, a second-order Taylor expansion of (4) around λ_0 yields $D_{\text{KL}} \approx \frac{1}{2} \Delta \lambda^\top H(\lambda_0) \Delta \lambda$, showing that the Fisher matrix H is the local metric tensor that governs infinitesimal output changes.

Concept probes and the pullback covector. A binary concept $W \in \{0, 1\}$ is detected by a linear probe $P(W = 1 | \lambda) = \sigma(\beta_W^\top \lambda + b_W)$ trained on the final hidden states, where $\beta_W \in \mathbb{R}^d$ is the probe weight vector. The first-order change in concept score induced by a perturbation δh at layer ℓ is

$$\Delta s_W = \beta_W^\top J \delta h + O(\|\delta h\|^2). \quad (5)$$

We call $q = J^\top \beta_W \in \mathbb{R}^d$ the *pullback covector* of the probe. It encodes, in the layer- ℓ activation space, the direction along which the concept score changes most rapidly.

We emphasize that q is a *covector* (dual vector): converting it into a tangent vector to be added to h requires raising the index via a metric, and the choice of metric is precisely the subject of this paper.

3 Pullback Fisher Metric for Intermediate Layers

This section develops the mathematical core of the paper. We derive the pullback Fisher metric and the closed-form optimal steering equation, establish the metric’s layer-wise recursive structure and spectral depth bounds, characterize when the resulting direction is globally versus locally optimal, extend the optimality to non-target KL under concept decomposability, and analyze the regularization scheme needed for practical computation.

3.1 The Optimal Steering Equation

We begin by asking: if one perturbs the layer- ℓ activation by δh , how much does the output distribution change? The answer defines the natural local metric on the activation space.

Theorem 3.1 (Pullback Fisher metric). *Let $h_0 \in \mathbb{R}^d$, $\lambda_0 = f^{(\ell)}(h_0)$, $J = Df^{(\ell)}(h_0) \in \mathbb{R}^{d \times d}$, and $H = H(\lambda_0) = \nabla^2 A(\lambda_0)$. If $f^{(\ell)}$ is C^2 and A is C^3 , then*

$$D_{\text{KL}}(P_{\lambda_0} \| P_{f(h_0 + \delta h)}) = \frac{1}{2} \delta h^\top \underbrace{J^\top H J}_{G^{(\ell)}(h_0)} \delta h + O(\|\delta h\|^3). \quad (6)$$

Proof. Write $\Delta\lambda = f(h_0 + \delta h) - \lambda_0 = J\delta h + O(\|\delta h\|^2)$. By the KL–Bregman identity from Section 2,

$$D_{\text{KL}} = \frac{1}{2} \Delta\lambda^\top H \Delta\lambda + O(\|\Delta\lambda\|^3).$$

Substituting $\Delta\lambda = J\delta h + O(\|\delta h\|^2)$ and absorbing cross terms yields (6). \square

The matrix $G^{(\ell)}(h_0) = J^\top H J$ is the *pullback Fisher metric*: a positive semidefinite, input-dependent, layer-specific Riemannian metric tensor on the intermediate activation space. It measures the second-order sensitivity of the output distribution to perturbations at layer ℓ . The general construction of pulling back a Riemannian metric through a smooth map is standard in differential geometry and has been applied to generative-model latent spaces; our contribution is its concrete instantiation for the Transformer residual stream with the softmax Fisher metric as the target-space geometry.

We note that, for softmax with cross-entropy loss, the Hessian of the per-sample loss $-\log P_\lambda(y)$ with respect to λ equals $H(\lambda)$ independently of the label y . Consequently, the pullback Fisher $G^{(\ell)} = J^\top H J$ coincides with the generalized Gauss–Newton (GGN) matrix of the loss with respect to intermediate activations, establishing a formal bridge between our information-geometric framework and the natural gradient optimization literature.

Given the metric, the optimal steering direction follows from a standard constrained minimization.

Theorem 3.2 (Closed-form optimal steering equation). *Let $G = G^{(\ell)}(h_0)$, $q = J^\top \beta_W$ be the pullback covector of the concept probe. If $q \in \text{Range}(G)$ and $q^\top G^+ q > 0$, then among all perturbations satisfying $q^\top \delta h = \rho$ (a prescribed first-order concept change), the unique minimizer of the second-order output KL $\frac{1}{2} \delta h^\top G \delta h$ with minimum Euclidean norm is*

$$\delta h^* = \frac{\rho}{q^\top G^+ q} G^+ q. \quad (7)$$

Equivalently, $G \delta h^* = \varepsilon J^\top \beta_W$ for $\varepsilon = \rho / (q^\top G^+ q)$.

Proof. The Lagrangian $\mathcal{L} = \frac{1}{2} \delta h^\top G \delta h - \eta (q^\top \delta h - \rho)$ yields the first-order condition $G \delta h = \eta q$. Since $q \in \text{Range}(G)$, the minimum-norm solution is $\delta h = \eta G^+ q$. The constraint $q^\top \delta h = \rho$ determines $\eta = \rho / (q^\top G^+ q)$. \square

Theorem 3.2 is the central practical result of this paper: it provides a *closed-form, one-step* steering equation. The Euclidean steering $\delta h \propto q$ corresponds to the special case $G = I$; the discrepancy between $G^+ q$ and q is precisely the “type error” of treating a covector as a tangent vector under the wrong metric.

3.2 Layer-wise Recursive Structure and Depth Bounds

The composite Jacobian $J = A_{L-1} \cdots A_\ell$ (cf. Section 2) endows $G^{(\ell)}$ with a natural recursive structure.

Theorem 3.3 (Recursive decomposition). $G^{(\ell)} = A_\ell^\top G^{(\ell+1)} A_\ell$.

Proof. By the chain rule, $J_{\ell \rightarrow L} = J_{\ell+1 \rightarrow L} A_\ell$. Then

$$G^{(\ell)} = (J_{\ell+1 \rightarrow L} A_\ell)^\top G^{(L)} (J_{\ell+1 \rightarrow L} A_\ell) = A_\ell^\top G^{(\ell+1)} A_\ell. \quad \square$$

This one-line identity has far-reaching consequences. Each residual block performs a congruence transformation on the metric, and the spectral properties of $A_\ell = I + DF_\ell$ control how much the geometry degrades with depth.

Theorem 3.4 (Condition number depth bound). *Let $A_k = I + B_k$ with $\|B_k\|_2 \leq \rho_k < 1$. Then*

$$\kappa(G^{(\ell)}) \leq \kappa(G^{(L)}) \prod_{k=\ell}^{L-1} \left(\frac{1 + \rho_k}{1 - \rho_k} \right)^2. \quad (8)$$

If $\rho_k \leq \rho$ for all k , then $\kappa(G^{(\ell)}) \leq \kappa(G^{(L)}) [(1 + \rho)/(1 - \rho)]^{2(L-\ell)}$.

Proof. By Theorem 3.3, $\kappa(G^{(\ell)}) \leq \kappa(G^{(\ell+1)}) \cdot \kappa(A_\ell)^2$. The residual structure gives

$$\sigma_{\max}(A_k) \leq 1 + \rho_k, \quad \sigma_{\min}(A_k) \geq 1 - \rho_k,$$

so $\kappa(A_k) \leq (1 + \rho_k)/(1 - \rho_k)$. The bound follows by induction. \square

Corollary 3.5 (Effective rank decay). *Define the trace effective rank $r_{\text{tr}}(G) = \text{tr}(G)/\lambda_{\max}(G)$. Then*

$$r_{\text{tr}}(G^{(\ell)}) \geq \frac{r_{\text{tr}}(G^{(\ell+1)})}{\kappa(A_\ell)^2}.$$

Proof. By Theorem 3.3, $\text{tr}(G^{(\ell)}) \geq \sigma_{\min}(A_\ell)^2 \text{tr}(G^{(\ell+1)})$ and $\lambda_{\max}(G^{(\ell)}) \leq \sigma_{\max}(A_\ell)^2 \lambda_{\max}(G^{(\ell+1)})$. Taking the ratio yields the bound. \square

Proposition 3.6 (Euclidean deviation identity). *The best scalar approximation to G satisfies*

$$\min_{c>0} \frac{\|G - cI\|_F}{\|G\|_F} = \sqrt{1 - \frac{\text{PR}(G)}{d}}, \quad (9)$$

where $\text{PR}(G) = (\text{tr } G)^2 / \text{tr}(G^2)$ is the participation ratio of the spectrum.

Proof. The minimizer is $c^* = \text{tr}(G)/d$. Expanding and simplifying,

$$\frac{\|G - c^*I\|_F^2}{\|G\|_F^2} = \frac{\text{tr}(G^2) - (\text{tr } G)^2/d}{\text{tr}(G^2)} = 1 - \frac{\text{PR}(G)}{d}.$$

Taking the square root gives the result. \square

The deviation identity converts the spectrum of G into a single number measuring how far the pullback geometry deviates from any isotropic Euclidean metric.

3.3 Global Optimality and Local Approximation Range

Theorems 3.1–3.2 establish local second-order optimality. Two natural questions arise: under what conditions does this extend to a global result, and how large is the “validity radius” of the local approximation?

Proposition 3.7 (Affine reachable global optimality). *If the remaining computation is affine in a neighborhood, $f(h) = \lambda_0 + J(h - h_0)$, then the reachable output set $\mathcal{S} = \lambda_0 + \text{Im}(J)$ is an affine subspace. The m -projection onto $\mathcal{S} \cap \{\lambda : \beta_W^\top \lambda = c\}$ satisfies the pullback dual condition*

$$J^\top(\phi(\hat{\lambda}) - \phi(\lambda_0)) = t J^\top \beta_W$$

for some $t \in \mathbb{R}$. Under small-step linearization $\phi(\hat{\lambda}) - \phi(\lambda_0) \approx HJ \delta h$, this reduces to $G \delta h = t q$, recovering Theorem 3.2.

Proof. The KKT conditions of the constrained minimization require the KL gradient to lie in the annihilator of the feasible tangent space:

$$\phi(\hat{\lambda}) - \phi(\lambda_0) \in (\text{Im}(J) \cap \ker(\beta_W^\top))^\perp = \text{Im}(J)^\perp + \text{span}\{\beta_W\}.$$

Left-multiplying by J^\top annihilates the $\text{Im}(J)^\perp$ component. Full proof in Appendix A. \square

For general nonlinear f , the local optimality direction G^+q is the first-order tangent to the global solution path: $\delta_*(\rho) = (\rho/(q^\top G^+q)) G^+q + O(\rho^2)$. A natural question is how quickly this approximation degrades. In Appendix A, we derive the explicit critical step size

$$r_{\text{crit}} = \min \left\{ \frac{\eta_{\text{KL}} m}{2 C_{\text{KL}}}, \sqrt{\frac{2 \eta_W |\rho|}{\|\beta_W\| K_2}} \right\}, \quad (10)$$

where $m = \lambda_{\min}^+(G)$, C_{KL} depends on the Jacobian and Fisher’s third-order constants, and $K_2 = \sup \|D^2 f\|_{\text{op}}$. Beyond r_{crit} , the KL value approximation degrades—but, remarkably, the direction remains accurate far beyond this radius.

Theorem 3.8 (Direction stability beyond the quadratic regime). *Assume $f \in C^2$, $\|G(h) - G(h_0)\|_2 \leq L_G \|h - h_0\|$ and $\|q(h) - q(h_0)\| \leq L_q \|h - h_0\|$ in a neighborhood of h_0 , and $\lambda_{\min}^+(G(h_0)) = m > 0$. Let $\delta_0(\rho)$ be the steering direction from Theorem 3.2, and $\delta_*(\rho)$ the true local KL minimizer under the exact nonlinear concept constraint. Then, for ρ sufficiently small,*

$$\delta_*(\rho) = \delta_0(\rho) + O(\rho^2), \quad 1 - \cos(\delta_*, \delta_0) = O(\rho^2). \quad (11)$$

Proof. The nonlinear KKT system for δ_* differs from the linearized system for δ_0 by $O(\|\delta\|^2)$ residuals. By the implicit function theorem, $(\delta_*(\rho), \nu_*(\rho))$ is C^1 in ρ with leading term $(\delta_0(\rho), \nu_0(\rho))$, giving $\|\delta_* - \delta_0\| = O(\rho^2)$. Since $\|\delta_0\| = \Theta(\rho)$, the unit-vector perturbation bound yields

$$\begin{aligned} 1 - \cos(\delta_*, \delta_0) &= \frac{1}{2} \left\| \frac{\delta_*}{\|\delta_*\|} - \frac{\delta_0}{\|\delta_0\|} \right\|^2 \\ &= O\left(\frac{\|\delta_* - \delta_0\|^2}{\|\delta_0\|^2}\right) = O(\rho^2). \end{aligned}$$

Full proof in Appendix B. \square

This result has a striking practical implication. The second-order KL approximation (6) incurs $O(\|\delta h\|^3)$ error, so its numerical accuracy degrades rapidly with step size. But the direction G^+q degrades only as $O(\rho^2)$ in cosine—much more slowly.

3.4 Non-target KL Optimality

Steering aims to change a target concept while preserving everything else. This requires decomposing the KL divergence into a concept component and a non-target component. We adopt a concept decomposability assumption.

Definition 3.9 (Concept decomposability). *Let counterfactual pairs $\mathcal{Y}_W = \{(y_i^0, y_i^1)\}_{i=1}^{n_W}$ define a binary concept W . The distribution P_λ is decomposable with respect to W if*

$$P_\lambda(y_i^w) = P_\lambda^W(w) P_\lambda^Z(z_i) \quad \text{for all } i, w,$$

where P_λ^W is a concept distribution over $\{0, 1\}$ and P_λ^Z is a non-target distribution over concept-neutral categories z_i .

Lemma 3.10 (Characterization of decomposability). *Let $d_i = \gamma_{y_i^1} - \gamma_{y_i^0}$ be the unembedding difference vector for the i -th counterfactual pair. Then P_λ is decomposable at λ if and only if $d_i^\top \lambda = d_j^\top \lambda$ for all pairs i, j .*

Proof. Decomposability requires the odds ratio $P_\lambda(y_i^1)/P_\lambda(y_i^0)$ to be independent of i . By the softmax parametrization, this ratio equals $\exp(d_i^\top \lambda)$, which is i -independent if and only if all $d_i^\top \lambda$ are equal. \square

Theorem 3.11 (Non-target KL optimality). *Let $\mathcal{A}_c = \{h : \beta_W^\top f(h) = c\}$. If $P_{f(h)}$ is decomposable with respect to W for all $h \in \mathcal{A}_c \cup \{h_0\}$, and $P_{f(h)}^W$ depends on h only through $\beta_W^\top f(h)$, then*

$$\arg \min_{h \in \mathcal{A}_c} D_{\text{KL}}(P_{f(h_0)} \| P_{f(h)}) \subseteq \arg \min_{h \in \mathcal{A}_c} D_{\text{KL}}(P_{f(h_0)}^Z \| P_{f(h)}^Z).$$

In particular, the direction from Theorem 3.2 locally minimizes both the total and the non-target KL to second order.

Proof. Under decomposability, the total KL decomposes as

$$D_{\text{KL}}(P \| Q) = \left(\sum_i P^Z(z_i) \right) D_{\text{KL}}(P^W \| Q^W) + D_{\text{KL}}(P^Z \| Q^Z).$$

On the constraint set \mathcal{A}_c , the concept score $\beta_W^\top f(h) = c$ is fixed, so P^W is constant and the first term does not vary. Thus minimizing total KL is equivalent to minimizing non-target KL. The argument extends to the second-order regime of Theorem 3.2 by applying the same decomposition to the quadratic form $\delta h^\top G \delta h$. Full proof in Appendix C. \square

When $\ell = L$, the feasible set \mathcal{A}_c reduces to an affine hyperplane in the output space and the theorem recovers the output-layer special case. For general $\ell < L$, the constraint set is defined through the nonlinear map $f^{(\ell)}$, and the optimality holds in the local second-order sense established by Theorem 3.2.

3.5 Adaptive Regularization

In practice, G is severely ill-conditioned, making direct computation of G^+q unstable. We use Tikhonov regularization $\delta_\alpha = (G + \alpha I)^{-1}q$, where $\alpha > 0$ is a damping parameter. The choice of α is critical.

Theorem 3.12 (Scale equivariance of adaptive regularization). *Let $\alpha(G) = c \cdot \lambda_{\text{med}}(G)$, where λ_{med} is the median positive eigenvalue and $c > 0$ is a fixed constant. If $\tilde{G} = sG$ for $s > 0$, then the normalized steering directions coincide:*

$$\begin{aligned} & \frac{(\tilde{G} + \alpha(\tilde{G})I)^{-1}q}{\|(\tilde{G} + \alpha(\tilde{G})I)^{-1}q\|} \\ &= \frac{(G + \alpha(G)I)^{-1}q}{\|(G + \alpha(G)I)^{-1}q\|}. \end{aligned} \quad (12)$$

Fixed α does not satisfy this property.

Proof. Since $\lambda_{\text{med}}(\tilde{G}) = s \lambda_{\text{med}}(G)$, we have $\alpha(\tilde{G}) = s \alpha(G)$, so

$$\tilde{G} + \alpha(\tilde{G})I = s(G + \alpha(G)I).$$

Inversion introduces a factor $1/s$ that cancels under normalization. \square

This property ensures that the steering direction is invariant to overall spectral scaling of G —a crucial requirement when steering across different layers whose metrics differ by orders of magnitude in scale but share similar spectral shape.

Theorem 3.13 (Tikhonov bias bound). *If $q \in \text{Range}(G)$ and λ_r is the smallest positive eigenvalue of G , then*

$$\|\delta_\alpha - G^+q\| \leq \frac{\alpha}{\lambda_r + \alpha} \|G^+q\|. \quad (13)$$

Proof. In the eigenbasis of G , the i -th component satisfies

$$\begin{aligned} (\delta_\alpha - G^+q)_i &= \frac{q_i}{\lambda_i + \alpha} - \frac{q_i}{\lambda_i} \\ &= -\frac{\alpha}{\lambda_i + \alpha} (G^+q)_i. \end{aligned}$$

Since $\alpha/(\lambda_i + \alpha) \leq \alpha/(\lambda_r + \alpha)$ for all i , the bound follows. \square

The bias is controlled by α/λ_r : as long as $\alpha \ll \lambda_r$, the regularized direction is close to the pseudoinverse direction. With G 's condition number at 10^7 , choosing $\alpha \sim \lambda_{\text{med}} \gg \lambda_r$ deliberately sacrifices accuracy in low-eigenvalue directions—but these directions have negligible Fisher cost (they barely affect the output), so the sacrifice is precisely where it matters least.

4 A Unified Framework for Steering Methods

The pullback Fisher metric $G = J^\top H J$ provides not only an optimal steering equation (Section 3) but also a principled lens through which every existing activation steering method can be analyzed. In this section we show that all linear steering methods implicitly adopt some metric M and some covector \hat{q} , and that the gap between their output KL and the Fisher optimum is precisely characterized by how M and \hat{q} deviate from the true G and q . This yields an exact, spectrally decomposed “excess KL budget” that explains when and why each method succeeds or fails.

Throughout this section, we work on the effective subspace S where $G|_S \succ 0$ (cf. Section 3.3). For notational simplicity, we write $G \succ 0$, understanding that all statements are restricted to S . The concept covector $q = J^\top \beta_W$ is assumed nonzero.

4.1 Excess KL and the Fisher-Pythagorean Decomposition

We first develop the general machinery for quantifying the excess output KL of any feasible steering direction relative to the Fisher optimum.

Definition 4.1 (Proxy metric steering). *Given a symmetric positive definite matrix $M \succ 0$ (the proxy metric) and a vector $\hat{q} \in \mathbb{R}^d$ (the proxy covector) satisfying $q^\top M^{-1} \hat{q} \neq 0$, the proxy metric steering direction is*

$$\delta_{M, \hat{q}}(\rho) = \frac{\rho M^{-1} \hat{q}}{q^\top M^{-1} \hat{q}}. \quad (14)$$

This direction satisfies the true concept constraint $q^\top \delta_{M, \hat{q}} = \rho$. The special case $\hat{q} = q$ gives

$$\delta_M(\rho) = \frac{\rho M^{-1} q}{q^\top M^{-1} q}, \quad (15)$$

which we call proxy metric steering with the correct covector. Setting $M = G$ and $\hat{q} = q$ recovers the Fisher-optimal direction δ_G^ from Theorem 3.2.*

The following identity is the foundation of the entire framework.

Theorem 4.2 (Fisher-Pythagorean excess cost identity). *Let δ_G^* be the Fisher-optimal direction (Theorem 3.2). For any $\tilde{\delta}$ satisfying the same concept constraint $q^\top \tilde{\delta} = \rho$,*

$$C_G(\tilde{\delta}) - C_G(\delta_G^*) = \frac{1}{2} (\tilde{\delta} - \delta_G^*)^\top G (\tilde{\delta} - \delta_G^*), \quad (16)$$

where $C_G(\delta) = \frac{1}{2} \delta^\top G \delta$ is the second-order output KL cost.

Proof. Let $e = \tilde{\delta} - \delta_G^*$. Since both $\tilde{\delta}$ and δ_G^* satisfy $q^\top \delta = \rho$, we have $q^\top e = 0$. By the KKT conditions of Theorem 3.2, there exists ν such that $G \delta_G^* = \nu q$, so $e^\top G \delta_G^* = \nu e^\top q = 0$. Expanding,

$$\begin{aligned} C_G(\tilde{\delta}) &= \frac{1}{2} (\delta_G^* + e)^\top G (\delta_G^* + e) \\ &= C_G(\delta_G^*) + e^\top G \delta_G^* + \frac{1}{2} e^\top G e \\ &= C_G(\delta_G^*) + \frac{1}{2} e^\top G e. \quad \square \end{aligned}$$

The identity (16) is *Pythagorean* in the G -inner product: the feasible affine hyperplane $\{q^\top \delta = \rho\}$ meets the ray through δ_G^* at a G -right angle. The excess cost is therefore the squared G -distance from $\tilde{\delta}$ to the optimum, measured in the Fisher geometry itself—not in Euclidean distance.

This identity has an immediate spectral refinement.

Theorem 4.3 (Spectral decomposition of excess KL). *Let $G = \sum_{i=1}^d \lambda_i u_i u_i^\top$ be the eigendecomposition of G . Define the error components $e_i = u_i^\top (\tilde{\delta} - \delta_G^*)$. Then*

$$C_G(\tilde{\delta}) - C_G(\delta_G^*) = \frac{1}{2} \sum_{i=1}^d \lambda_i e_i^2. \quad (17)$$

Proof. By Theorem 4.2, the excess cost equals $\frac{1}{2} e^\top G e$. Substituting the eigendecomposition of G gives $e^\top G e = \sum_{i=1}^d \lambda_i (u_i^\top e)^2 = \sum_{i=1}^d \lambda_i e_i^2$. \square

Corollary 4.4 (Low-curvature errors are KL-invisible). *If the error $e = \tilde{\delta} - \delta_G^*$ is orthogonal to the top- k eigenvectors of G (i.e., $e_i = 0$ for $i = 1, \dots, k$, where eigenvalues are ordered $\lambda_1 \geq \dots \geq \lambda_d$), then*

$$C_G(\tilde{\delta}) - C_G(\delta_G^*) \leq \frac{1}{2} \lambda_{k+1} \|e\|^2.$$

Proof. Dropping the zero terms, $\sum_{i=k+1}^d \lambda_i e_i^2 \leq \lambda_{k+1} \sum_{i=k+1}^d e_i^2 \leq \lambda_{k+1} \|e\|^2$. \square

Corollary 4.4 reveals a fundamental asymmetry: errors in directions of high Fisher curvature are expensive; errors in directions of low curvature are nearly free. A method can be far from δ_G^* in Euclidean distance yet incur negligible excess KL, provided its errors concentrate in low-eigenvalue directions. This explains why Euclidean methods sometimes perform adequately despite using the wrong metric.

We now derive the exact cost of proxy metric steering.

Theorem 4.5 (Cost of proxy metric steering). *Let $M \succ 0$ and $\hat{q} = q$ (correct covector). The second-order KL cost of δ_M is*

$$C_G(\delta_M) = \frac{\rho^2}{2} \frac{q^\top M^{-1} G M^{-1} q}{(q^\top M^{-1} q)^2}, \quad (18)$$

and the cost ratio relative to the Fisher optimum is

$$R_G(M; q) = \frac{C_G(\delta_M)}{C_G(\delta_G^*)} = \frac{q^\top M^{-1} G M^{-1} q}{(q^\top M^{-1} q)^2} \cdot (q^\top G^{-1} q). \quad (19)$$

Moreover, $R_G(M; q) \geq 1$, with equality if and only if $\delta_M = \delta_G^*$.

Proof. Substituting $\delta_M = \rho M^{-1} q / (q^\top M^{-1} q)$ into $C_G(\delta) = \frac{1}{2} \delta^\top G \delta$ gives (18) directly. Dividing by $C_G(\delta_G^*) = \rho^2 / (2 q^\top G^{-1} q)$ yields (19). The inequality $R_G \geq 1$ follows from the optimality of δ_G^* . \square

The cost ratio admits a revealing spectral characterization.

Theorem 4.6 (Cost ratio as weighted coefficient of variation). *Define the whitened matrix*

$$B = G^{1/2} M^{-1} G^{1/2}$$

and the unit direction

$$\nu = \frac{G^{-1/2} q}{\|G^{-1/2} q\|} = \frac{G^{-1/2} q}{\sqrt{q^\top G^{-1} q}}.$$

Let $B = \sum_i b_i r_i r_i^\top$ be the eigendecomposition of B , and define weights $w_i = (r_i^\top \nu)^2$. Then

$$R_G(M; q) = \frac{\nu^\top B^2 \nu}{(\nu^\top B \nu)^2} = \frac{\sum_i w_i b_i^2}{(\sum_i w_i b_i)^2} = 1 + \frac{\text{Var}_w(b)}{(\mathbb{E}_w[b])^2}, \quad (20)$$

where $\mathbb{E}_w[b] = \sum_i w_i b_i$ and $\text{Var}_w(b) = \sum_i w_i b_i^2 - (\sum_i w_i b_i)^2$.

Proof. Substituting $q = G^{1/2} (G^{-1/2} q)$, we compute

$$\begin{aligned} q^\top M^{-1} q &= (G^{-1/2} q)^\top G^{1/2} M^{-1} G^{1/2} (G^{-1/2} q) \\ &= (q^\top G^{-1} q) \nu^\top B \nu. \end{aligned}$$

Similarly,

$$\begin{aligned} q^\top M^{-1} G M^{-1} q &= (G^{-1/2} q)^\top (G^{1/2} M^{-1} G^{1/2})^2 (G^{-1/2} q) \\ &= (q^\top G^{-1} q) \nu^\top B^2 \nu, \end{aligned}$$

where we used $G^{1/2} M^{-1} G M^{-1} G^{1/2} = B^2$. Substituting into (19),

$$R_G(M; q) = \frac{(q^\top G^{-1} q) \nu^\top B^2 \nu}{[(q^\top G^{-1} q) \nu^\top B \nu]^2} (q^\top G^{-1} q) = \frac{\nu^\top B^2 \nu}{(\nu^\top B \nu)^2}.$$

Expanding in the eigenbasis of B and writing $\mathbb{E}_w[b^2] / (\mathbb{E}_w[b])^2 = 1 + \text{Var}_w(b) / (\mathbb{E}_w[b])^2$ completes the proof. \square

Theorem 4.6 gives the central interpretive insight of the framework: *the cost ratio of a proxy metric method is not determined by how far M is from G in any matrix norm, but by how variable the whitened scaling $B = G^{1/2}M^{-1}G^{1/2}$ appears along the concept-relevant direction ν . If B acts as a near-constant scalar on ν , then $\text{Var}_w(b) \approx 0$ and $R_G \approx 1$, even if M differs wildly from G in other directions. Conversely, a small metric error that creates spectral variation along ν can cause substantial excess KL.*

Corollary 4.7 (Stability under relative perturbation). *If $\|G^{-1/2}(M - G)G^{-1/2}\|_2 \leq \eta < 1$, then*

$$R_G(M; q) \leq \frac{1}{1 - \eta^2}. \quad (21)$$

Proof. Let $S = G^{-1/2}(M - G)G^{-1/2}$, so $M = G^{1/2}(I + S)G^{1/2}$. Since $\|S\|_2 \leq \eta < 1$, we have $B = G^{1/2}M^{-1}G^{1/2} = (I + S)^{-1}$, whose eigenvalues lie in $[1/(1 + \eta), 1/(1 - \eta)]$. By the Kantorovich inequality, for any unit vector ν and any B with spectrum in $[a, b]$,

$$\frac{\nu^\top B^2 \nu}{(\nu^\top B \nu)^2} \leq \frac{(a + b)^2}{4ab}.$$

Substituting $a = 1/(1 + \eta)$ and $b = 1/(1 - \eta)$ gives $(a + b)^2/(4ab) = 1/(1 - \eta^2)$. \square

4.2 Implicit Metrics of Existing Methods

We now show that every prominent steering method fits the proxy metric template (Definition 4.1), and identify each method’s implicit metric M and covector \hat{q} .

Remark 4.8 (Universality and non-uniqueness of implicit metrics). *For any direction v with $q^\top v > 0$, there exist infinitely many $M \succ 0$ satisfying $M^{-1}q \propto v$. (Simply solve $Mv = q$ for symmetric positive definite M ; the solution is non-unique.) Therefore, the proxy metric representation $\delta \propto M^{-1}q$ is universal—every successful steering direction admits one—but not identifying: it does not uniquely determine M . When a method provides only a direction v without further structure, we adopt the canonical representation $M = I$, $\hat{q} = v$. An informative metric identification is only possible when the method comes with additional distributional or structural assumptions.*

Table 1 summarizes the implicit metrics and covectors of major steering methods. Both ActAdd (Turner et al. 2024) and CAA (Rimsky et al. 2024) use the Euclidean metric $M = I$ but differ in their covectors: ActAdd computes a steering vector from a single pair of contrastive prompts, while CAA averages over hundreds of contrastive pairs, yielding the population mean difference $\mu_+ - \mu_-$. This averaging has a precise consequence in our framework: under a shared-covariance Gaussian model for the activations, CAA’s covector admits a closed-form identification with the true concept covector q .

Table 1: Existing steering methods as proxy metric operations. $G = J^\top H J$, $q = J^\top \beta_W$.

Method	Metric M	Covector \hat{q}
ActAdd	I	$h(p^+) - h(p^-)$
CAA	I	$\mu_+ - \mu_-$
ITI	D^{-1} (diag.)	q
Rep. Surgery	Σ^{-1}	context-dep.
K-FAC	$B \otimes A$	q
Ours	$J^\top H J$	$J^\top \beta_W$

Proposition 4.9 (CAA under shared-covariance Gaussian model). *Suppose the layer- ℓ activations of the two concept classes follow $h \mid W = w \sim \mathcal{N}(\mu_w, \Sigma)$ with shared covariance. Then the optimal linear probe is $q = \Sigma^{-1}(\mu_1 - \mu_0)$, and the CAA mean-difference vector satisfies $v_{\text{CAA}} = \mu_1 - \mu_0 = \Sigma q$. Hence*

$$\delta_{\text{CAA}} = \frac{\rho v_{\text{CAA}}}{q^\top v_{\text{CAA}}} = \frac{\rho \Sigma q}{q^\top \Sigma q} = \delta_{\Sigma^{-1}}(\rho),$$

i.e., CAA implicitly uses the proxy metric $M = \Sigma^{-1}$ (the precision matrix of the activation distribution).

Proof. By Fisher linear discriminant analysis, the Bayes-optimal linear classifier direction in the shared-covariance Gaussian model is $q = \Sigma^{-1}(\mu_1 - \mu_0)$, hence $\mu_1 - \mu_0 = \Sigma q$. The CAA steering direction $\delta_{\text{CAA}} \propto v_{\text{CAA}} = \Sigma q$ then matches δ_M with $M = \Sigma^{-1}$, since $M^{-1}q = \Sigma q$. \square

The excess KL of CAA relative to the Fisher optimum is therefore governed by how closely the activation precision matrix Σ^{-1} approximates the pullback Fisher G . These two matrices arise from fundamentally different quantities: Σ^{-1} captures the *statistical variability* of activations across data, while $G = J^\top H J$ captures the *sensitivity* of the output distribution to activation perturbations. They coincide only under restrictive conditions (e.g., if the data covariance and the Fisher metric share the same eigenvectors with proportional eigenvalues).

Proposition 4.10 (ITI subspace restriction cost). *Let $S \subseteq \mathbb{R}^d$ be a k -dimensional subspace (e.g., the span of selected attention head outputs), with orthonormal basis $\Psi \in \mathbb{R}^{d \times k}$. Define the restricted metric $G_S = \Psi^\top G \Psi \in \mathbb{R}^{k \times k}$ and the restricted covector $q_S = \Psi^\top q \in \mathbb{R}^k$. The Fisher-optimal direction within S is*

$$\delta_S^* = \frac{\rho \Psi G_S^{-1} q_S}{q_S^\top G_S^{-1} q_S},$$

with cost

$$C_G(\delta_S^*) = \frac{\rho^2}{2 q_S^\top G_S^{-1} q_S}. \quad (22)$$

The excess KL of ITI decomposes as

$$\underbrace{C_G(\delta_{\text{ITI}}) - C_G(\delta_G^*)}_{\text{total excess}} = \underbrace{C_G(\delta_S^*) - C_G(\delta_G^*)}_{\text{subspace restriction cost}} + \underbrace{C_G(\delta_{\text{ITI}}) - C_G(\delta_S^*)}_{\text{within-}S \text{ metric error}}. \quad (23)$$

The subspace restriction cost is

$$C_G(\delta_S^*) - C_G(\delta_G^*) = \frac{\rho^2}{2} \left(\frac{1}{q_S^\top G_S^{-1} q_S} - \frac{1}{q^\top G^{-1} q} \right) \geq 0. \quad (24)$$

This term is zero if and only if $\delta_G^* \in S$.

Proof. The direction δ_S^* solves $\min_{\delta \in S} \frac{1}{2} \delta^\top G \delta$ subject to $q^\top \delta = \rho$. Writing $\delta = \Psi \alpha$ transforms this into

$$\min_{\alpha} \frac{1}{2} \alpha^\top G_S \alpha \quad \text{s.t.} \quad q_S^\top \alpha = \rho,$$

whose solution is $\alpha^* = \rho G_S^{-1} q_S / (q_S^\top G_S^{-1} q_S)$, giving δ_S^* and cost (22). The decomposition (23) follows by adding and subtracting $C_G(\delta_S^*)$. The non-negativity of (24) follows from $q_S^\top G_S^{-1} q_S \leq q^\top G^{-1} q$ (restricting the feasible set can only increase the optimum), with equality iff $G^{-1} q \in S$. \square

The decomposition (23) reveals that ITI pays two distinct costs: the *subspace restriction cost*, which is unavoidable once the head subspace S is fixed, and the *within-subspace metric error*, which arises from ITI’s use of a diagonal or identity metric within S instead of the restricted Fisher G_S .

For the remaining methods in Table 1: **Representation Surgery** uses the base-class inverse covariance Σ_-^{-1} as its proxy metric, and in general also introduces a context-dependent covector error; its analysis follows Theorem 4.5 with $M = \Sigma_-^{-1}$. **K-FAC** replaces G by a Kronecker product $B \otimes A$, discarding cross-block Fisher coupling. In each case, the cost ratio (19) applies with the appropriate (M, \hat{q}) .

4.3 Cost Ratio Bounds and Method Ranking

We now turn to bounding the cost ratio and understanding when one method provably outperforms another.

Theorem 4.11 (Kantorovich bound for Euclidean steering). *The cost ratio of Euclidean steering ($M = I, \hat{q} = q$) satisfies*

$$1 \leq R_G(I; q) = \frac{(q^\top G q)(q^\top G^{-1} q)}{\|q\|^4} \leq \frac{(\kappa(G) + 1)^2}{4 \kappa(G)}, \quad (25)$$

where $\kappa(G) = \lambda_{\max}(G) / \lambda_{\min}(G)$ is the condition number. The lower bound is achieved when q is an eigenvector of G ; the upper bound is achieved when q has equal projections onto the eigenvectors of the largest and smallest eigenvalues.

Proof. With $M = I$, the cost formula (18) gives $C_G(\delta_I) = \rho^2 (q^\top G q) / (2 \|q\|^4)$. Dividing by $C_G(\delta_G^*) = \rho^2 / (2 q^\top G^{-1} q)$ yields the middle expression. The lower bound $R_G \geq 1$ follows from the Cauchy–Schwarz inequality applied to $G^{1/2} q$ and $G^{-1/2} q$:

$$(q^\top G q)(q^\top G^{-1} q) = \|G^{1/2} q\|^2 \|G^{-1/2} q\|^2 \geq (q^\top q)^2 = \|q\|^4.$$

The upper bound is the classical Kantorovich inequality: for G with eigenvalues in $[\lambda_{\min}, \lambda_{\max}]$,

$$(q^\top G q)(q^\top G^{-1} q) \leq \frac{(\lambda_{\max} + \lambda_{\min})^2}{4 \lambda_{\max} \lambda_{\min}} \|q\|^4 = \frac{(\kappa + 1)^2}{4 \kappa} \|q\|^4. \quad \square$$

This bound connects the condition number of G —a quantity measured in Section 3.2—directly to the potential gain of Fisher steering over Euclidean steering. A large $\kappa(G)$ means the Euclidean method is potentially wasting a large fraction of its “perturbation budget” on directions with high Fisher curvature, while achieving little concept change. Whether the potential is realized depends on the alignment of q with the eigenspectrum of G .

Theorem 4.12 (Information-theoretic lower bound). *If a method has access only to the covector q and the Euclidean inner product, and must produce a direction equivariant under orthogonal transformations, then the only feasible direction is $\delta \propto q$. The unavoidable excess cost is*

$$C_G(\delta_I) - C_G(\delta_G^*) = \frac{\rho^2}{2} \left(\frac{q^\top G q}{\|q\|^4} - \frac{1}{q^\top G^{-1} q} \right). \quad (26)$$

This excess vanishes if and only if q is an eigenvector of G .

Proof. Rotational equivariance requires the direction to be a function of q alone that commutes with orthogonal transformations, forcing $\delta \propto q$. The normalized solution is $\delta_I = \rho q / \|q\|^2$. The excess cost follows from subtracting $C_G(\delta_G^*) = \rho^2 / (2 q^\top G^{-1} q)$ from $C_G(\delta_I) = \rho^2 (q^\top G q) / (2 \|q\|^4)$. For the vanishing condition: writing $q = \sum_i q_i u_i$ in the eigenbasis of G , the excess is $\frac{\rho^2}{2} [\sum_i \lambda_i q_i^2 / (\sum_i q_i^2)^2 - 1 / \sum_i q_i^2 / \lambda_i]$. This is zero iff λ_i is constant on the support of q , i.e., iff q lies in an eigenspace of G . \square

Theorem 4.12 quantifies the fundamental cost of geometric ignorance: without knowledge of G , a method using only the concept direction q must pay a penalty determined by how much G rotates q relative to the identity. This motivates methods that estimate or approximate G .

We next address the question of whether the matrix distance $\|M - G\|$ can serve as a proxy for method quality.

Proposition 4.13 (Ranking by matrix norm is generally invalid). *There exist G, q, M_A, M_B such that $\|M_A - G\|_2 < \|M_B - G\|_2$ but $C_G(\delta_{M_A}) > C_G(\delta_{M_B})$.*

Proof. Take $d = 2, G = I, q = e_1, M_B = \text{diag}(1, K)$ with $K \gg 1$, and

$$M_A = \begin{pmatrix} 1 & \epsilon \\ \epsilon & 1 \end{pmatrix}, \quad 0 < \epsilon < 1.$$

Then $\|M_A - I\|_2 = \epsilon < K - 1 = \|M_B - I\|_2$ for $\epsilon < K - 1$. But $M_B^{-1} q = e_1 = \delta_G^* / \rho$, giving $C_G(\delta_{M_B}) = \rho^2 / 2$. Meanwhile, $M_A^{-1} e_1 = (1, -\epsilon)^\top / (1 - \epsilon^2)$, so $\delta_{M_A} = \rho(1, -\epsilon)^\top$ and $C_G(\delta_{M_A}) = \rho^2(1 + \epsilon^2) / 2 > C_G(\delta_{M_B})$. \square

The failure occurs because M_B ’s large error in the e_2 direction is invisible to the concept $q = e_1$, while M_A ’s small off-diagonal error leaks directly into the concept direction. The correct ranking criterion involves the concept-weighted spectral structure.

Theorem 4.14 (Correct method ranking condition). *For two proxy metrics $M_A, M_B \succ 0$ with corresponding whitened matrices $B_A = G^{1/2} M_A^{-1} G^{1/2}$ and $B_B = G^{1/2} M_B^{-1} G^{1/2}$, the ranking $C_G(\delta_{M_A}) \leq C_G(\delta_{M_B})$ holds if and only if*

$$\frac{\text{Var}_\nu(B_A)}{(\mathbb{E}_\nu[B_A])^2} \leq \frac{\text{Var}_\nu(B_B)}{(\mathbb{E}_\nu[B_B])^2}, \quad (27)$$

where $\nu = G^{-1/2} q / \|G^{-1/2} q\|$ and the variance and expectation are computed as in Theorem 4.6.

Proof. By Theorem 4.6, $R_G(M; q) = 1 + \text{Var}_\nu(B) / (\mathbb{E}_\nu[B])^2$. Since $C_G(\delta_M) = R_G(M; q) \cdot C_G(\delta_G^*)$ and $C_G(\delta_G^*) > 0$, the ranking of costs is equivalent to the ranking of cost ratios, which is equivalent to (27). \square

In other words, the method whose whitened scaling matrix has the smaller *coefficient of variation* along the concept direction is provably better, regardless of what happens in concept-orthogonal directions.

We close the section with an analysis of diagonal approximations, which are the simplest nontrivial improvement over Euclidean steering.

Proposition 4.15 (Diagonal Fisher cost). *Let $D = \text{diag}(G)$ and $E = G - D$, so that $G = D + E$. Define $z = D^{-1/2} q$ and $\tilde{B} = D^{-1/2} G D^{-1/2} = I + D^{-1/2} E D^{-1/2}$. The diagonal Fisher steering $\delta_D = \rho D^{-1} q / (q^\top D^{-1} q)$ has cost*

$$C_G(\delta_D) = \frac{\rho^2}{2} \frac{z^\top \tilde{B} z}{(z^\top z)^2}, \quad (28)$$

and cost ratio

$$R_D = \frac{(z^\top \tilde{B} z) (z^\top \tilde{B}^{-1} z)}{(z^\top z)^2}. \quad (29)$$

If $\|D^{-1/2} E D^{-1/2}\|_2 \leq \eta < 1$, then $R_D \leq (1 + \eta) / (1 - \eta)$.

Proof. By Theorem 4.5 with $M = D$: $C_G(\delta_D) = \rho^2 q^\top D^{-1} G D^{-1} q / (2(q^\top D^{-1} q)^2)$. Substituting $z = D^{-1/2} q$ gives $q^\top D^{-1} q = z^\top z$ and $q^\top D^{-1} G D^{-1} q = z^\top \tilde{B} z$, yielding (28). Similarly, $q^\top G^{-1} q = z^\top \tilde{B}^{-1} z$, giving (29).

For the bound: \tilde{B} has eigenvalues in $[1 - \eta, 1 + \eta]$, so $z^\top \tilde{B} z \leq (1 + \eta) z^\top z$ and $z^\top \tilde{B}^{-1} z \leq z^\top z / (1 - \eta)$. Thus $R_D \leq (1 + \eta) / (1 - \eta)$. \square

The diagonal approximation is effective when the off-diagonal elements of the Fisher metric, measured in the scale $D^{-1/2} E D^{-1/2}$, are small. However, even small off-diagonal Fisher coupling along the concept direction can cause nontrivial excess KL, as the following negative result shows.

Proposition 4.16 (No universal lower bound from off-diagonal energy). *There is no function $f : \mathbb{R}_+ \rightarrow \mathbb{R}_+$ with $f(\eta) > 0$ for $\eta > 0$ such that $R_D - 1 \geq f(\|D^{-1/2} E D^{-1/2}\|_2)$ holds for all q .*

Proof. Take $d = 2$, $G = \begin{pmatrix} 1 & \epsilon \\ \epsilon & 1 \end{pmatrix}$, so $D = I$ and $E = \begin{pmatrix} 0 & \epsilon \\ \epsilon & 0 \end{pmatrix}$ with $\|D^{-1/2} E D^{-1/2}\|_2 = \epsilon > 0$. Let $q = (1, 1)^\top / \sqrt{2}$, which is an eigenvector of G with eigenvalue $1 + \epsilon$. Then $D^{-1} q = q$ and $G^{-1} q = q / (1 + \epsilon)$, so $\delta_D = \delta_G^* = \rho q$ and $R_D = 1$ despite $E \neq 0$. \square

This confirms that the impact of metric approximation errors on steering quality is fundamentally direction-dependent: it is the interplay between the concept covector q and the error structure E that determines the cost, not the error magnitude alone.

5 Experiments

We validate our theoretical framework through three groups of experiments on GPT-2 small (Radford et al. 2019) (124M parameters, $L = 12$ layers, $d = 768$). Experiment 1 (§5.1) verifies the direction stability theorem on controlled toy models. Experiment 2 (§5.2) quantifies the pullback Fisher metric’s spectral properties, confirming the failure of the Euclidean assumption. Experiment 3 (§5.3) compares iterative Fisher steering against four baselines using an exact equal-probability evaluation framework.

5.1 Experiment 1: Direction Stability on Toy Models

We first verify Theorem 3.8 in a controlled setting where the exact Jacobian and Fisher metric can be computed without approximation.

Setup. We construct three random Transformer-like toy models (hidden dimensions $d \in \{4, 8, 16\}$, denoted *tiny*, *small*, and *medium*), each consisting of a random affine map followed by softmax over $|\mathcal{Y}| = 2d$ categories. For each configuration, we sample 300 random inputs and compute the exact pullback Fisher metric G , the Fisher-optimal direction $\delta_{\text{nat}} = G^{-1} q / \|G^{-1} q\|$, and the numerically exact KL-minimizing direction δ_{exact} via grid search over the concept constraint hyperplane. We then compare: (a) the directional alignment $\cos(\delta_{\text{nat}}, \delta_{\text{exact}})$ as a function of the concept change ρ ; (b) the KL ratio $R_{\text{KL}} = D_{\text{KL}}^{\text{euc}} / D_{\text{KL}}^{\text{nat}}$ at equal concept change.

Results. Across all configurations, the Fisher-optimal direction achieves a median cosine similarity of > 0.997 with the exact KL-minimizing direction, even when the step size exceeds the KL approximation’s critical radius r_{crit} by 80–1000 \times (Figure 1a). This directly validates Theorem 3.8: the direction’s validity range is fundamentally larger than the KL value’s validity range.

The KL ratio R_{KL} at $\rho = 0.1$ has a median of 1.82 across all 900 cases (Figure 1b), indicating that Euclidean steering incurs 82% more output distortion than Fisher steering at matched concept change. The overall Spearman correlation between $\kappa(G)$ and R_{KL} is $r = 0.502$ ($p < 10^{-56}$), confirming that the advantage of Fisher steering grows with geometric anisotropy, as predicted by Theorem 4.11.

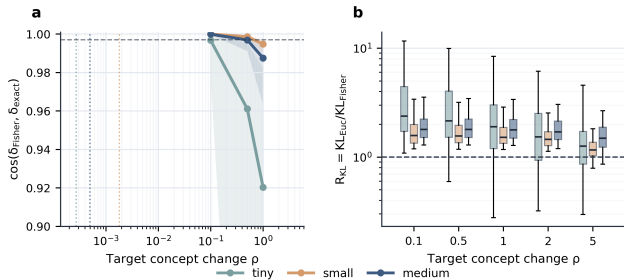


Figure 1: Direction stability on toy models. **(a)** Cosine similarity between the Fisher-optimal direction and the numerically exact KL-minimizing direction as a function of the target concept change ρ . Vertical dotted lines mark the critical radius r_{crit} of the second-order KL approximation for each configuration. The Fisher direction remains highly aligned (> 0.92) even far beyond r_{crit} , validating Theorem 3.8. **(b)** KL ratio $R_{\text{KL}} = D_{\text{KL}}^{\text{euc}} / D_{\text{KL}}^{\text{Fisher}}$ at matched concept change. All medians exceed 1, confirming that Fisher steering consistently incurs less output distortion than Euclidean steering. Results aggregated over 300 random inputs per configuration.

5.2 Experiment 2: Intermediate-Layer Geometry of GPT-2

Setup. For the concept `verb_third` (verb base form \rightarrow third-person singular, e.g., `run` \rightarrow `runs`), we compute the exact pullback Fisher metric $G^{(\ell)} = J^T H J$ at four layers ($\ell \in \{3, 6, 9, 11\}$) across 100 test contexts drawn from the C4 validation set (Raffel et al. 2020). The Jacobian $J = Df^{(\ell)}$ is computed via 768 backward passes through the hook-based forward function, and the Fisher H is computed from the top-5000 tokens by probability mass.

Results. Table 2 summarizes the spectral properties of G . The condition number exceeds 10^7 at all layers, growing from 4.9×10^7 at $\ell = 11$ to 9.5×10^7 at $\ell = 3$ —consistent with the exponential depth bound of Theorem 3.4 with a per-layer factor of ≈ 1.09 . The effective rank (Shannon entropy of the normalized eigenvalue distribution) ranges from 2.4% to 17.1% of the ambient 768 dimensions. The Euclidean deviation (Proposition 3.6) exceeds 97% at all layers: *no scalar multiple of the identity matrix can approximate the pullback Fisher to within 3% relative error.*

Table 2: Spectral properties of the pullback Fisher metric $G^{(\ell)}$ on GPT-2 small (median over 100 contexts, `verb_third`).

	Layer 3	Layer 6	Layer 9	Layer 11
$\kappa(G)$	9.5×10^7	7.1×10^7	5.0×10^7	4.9×10^7
Eff. rank / d	2.4%	3.7%	15.2%	17.1%
Null dim.	62	11	7	7
Deviation	99.6%	99.4%	97.8%	98.0%

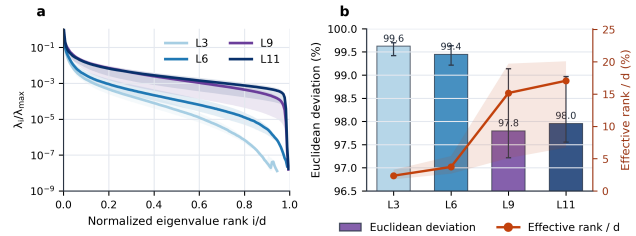


Figure 2: Pullback Fisher geometry of GPT-2 intermediate layers. **(a)** Normalized eigenvalue spectrum $\lambda_i / \lambda_{\text{max}}$ of $G^{(\ell)}$ at four layers (median over 100 contexts, `verb_third`). The spectrum spans over 7 orders of magnitude, confirming extreme anisotropy. **(b)** Euclidean deviation (bars, left axis) and effective rank as a fraction of the ambient dimension (line, right axis). All layers exhibit deviation $> 97\%$, meaning no isotropic Euclidean metric can approximate the pullback Fisher to within 3% relative error.

5.3 Experiment 3: Iterative Fisher Steering on GPT-2

Experimental Design We adopt the counterfactual concept evaluation framework of Park et al. (2026), which provides a rigorous, distribution-level criterion for measuring steering quality. In this framework, a binary concept $W \in \{0, 1\}$ is defined by a set of *counterfactual token pairs* $\{(y_i^0, y_i^1)\}_{i=1}^{n_W}$, where y_i^0 and y_i^1 differ only in the target concept (e.g., `run` vs. `runs` for the third-person concept). Given a context where the model predicts tokens from these pairs, the *concept probability* is defined as

$$P^W(1) = \frac{\sum_{i=1}^{n_W} P(y_i^1)}{\sum_{i=1}^{n_W} P(y_i^0) + \sum_{i=1}^{n_W} P(y_i^1)}, \quad (30)$$

where $P(y) = P_\lambda(y)$ is the model’s output probability for token y . The goal of steering is to increase $P^W(1)$ from an initial value (typically $\ll 0.5$ for base contexts) toward a target level (e.g., 0.9), while minimizing disruption to the rest of the output distribution.

Concepts. Following Park et al. (2026), we construct counterfactual pairs for three English verb-morphology concepts:

- `verb_third`: base form \rightarrow third-person singular (`run` \rightarrow `runs`, `make` \rightarrow `makes`, ...)
- `verb_ing`: base form \rightarrow progressive (`run` \rightarrow `running`, `make` \rightarrow `making`, ...)
- `verb_past`: base form \rightarrow past tense (`run` \rightarrow `ran`, `go` \rightarrow `went`, ...)

Only pairs where both forms are single tokens in GPT-2’s vocabulary are retained. Contexts are drawn from the C4 validation set (Raffel et al. 2020) and filtered by the Top-3 criterion of Park et al. (2026): for each token position, we require that the model’s top-3 predictions by probability all belong to either the base set $\{y_i^0\}$ or the target set $\{y_i^1\}$, with cumulative probability ≥ 0.7 . This ensures that the concept is well-defined at the selected position. Each concept yields approximately 200 training contexts and 25 test contexts, with strict separation.

Evaluation Metrics A key insight from Park et al. (2026) is that the standard KL divergence $D_{\text{KL}}(P_{\text{orig}} \| P_{\text{steered}})$ conflates two distinct effects: the intended concept change and the unintended disruption to other aspects of the distribution. To disentangle them, we adopt Park et al.’s *concept-decomposed* evaluation, which splits the output distribution into a concept component and a non-target component.

Specifically, we partition the vocabulary into concept-relevant groups $\{(y_i^0, y_i^1)\}$ and the remaining tokens $\mathcal{Y}_{\text{rest}}$. The *off-target distribution* P^Z is defined over the concept-neutral categories z_i (each z_i merging the pair (y_i^0, y_i^1) into a single category) plus each individual token in $\mathcal{Y}_{\text{rest}}$:

$$P^Z(z_i) = P(y_i^0) + P(y_i^1), \quad P^Z(y) = P(y) \text{ for } y \in \mathcal{Y}_{\text{rest}}. \quad (31)$$

The *off-target KL divergence* is then

$$D_{\text{KL}}^{\text{off}} = D_{\text{KL}}(P_{\text{orig}}^Z \| P_{\text{steered}}^Z) = \sum_z P_{\text{orig}}^Z(z) \log \frac{P_{\text{orig}}^Z(z)}{P_{\text{steered}}^Z(z)}. \quad (32)$$

This quantity measures how much the steered distribution disturbs the model’s predictions *beyond* the intended concept change. A method that cleanly shifts P^W without affecting P^Z achieves $D_{\text{KL}}^{\text{off}} = 0$. Our Theorem 3.11 predicts that the Fisher-optimal direction minimizes exactly this quantity (to second order) under concept decomposability.

We additionally report the *counterfactual mass preservation*: the ratio $\sum_i P_{\text{steered}}(y_i^0) + P_{\text{steered}}(y_i^1)$ divided by the corresponding sum under P_{orig} . Values close to 1 indicate that the steered distribution retains probability mass on the concept-relevant tokens rather than leaking it to unrelated tokens.

Methods Our method: Iterative Fisher steering. Two considerations motivate an iterative approach rather than a single-step application of Theorem 3.2. First, the pull-back covector $q = J^\top \beta_W$ of a linear probe is not well-aligned with the nonlinear concept probability $P^W(1)$: stepping along $J^\top \beta_W$ produces only marginal changes in $P^W(1)$, motivating the use of the concept probability gradient $\nabla_h P^W(1)$ as the covector. Second, the condition number of 10^7 creates a tension between directional optimality and concept efficiency in a single step, which iterative application naturally resolves by accumulating many small Fisher-optimal steps.

The full procedure is summarized in Algorithm 1. At each step t , we compute the concept gradient covector $q_t = \nabla_h P^W(1)|_{h_t}$ (one backward pass), update the Fisher matrix $H_t = \nabla^2 A(\lambda_t)$ from the current output probabilities (one forward pass), assemble $G_t = J_0^\top H_t J_0$ using the Jacobian J_0 frozen at the initial point, apply adaptive Tikhonov regularization $\alpha_t = \lambda_{\text{med}}(G_t)$ (Theorem 3.12), and step along the normalized direction $(G_t + \alpha_t I)^{-1} q_t$. The Jacobian J_0 is computed once per context (≈ 15 seconds); each subsequent step costs ≈ 1.5 seconds.

Using $q_t = \nabla_h P^W(1)$ does not affect any theorem—the optimality of $(G + \alpha I)^{-1} q$ holds for any covector q . The change is purely empirical: $\nabla_h P^W(1)$ directly targets the quantity of interest, while $J^\top \beta_W$ targets a linear proxy.

Algorithm 1: Iterative Fisher Steering at Layer ℓ

Require: Model f , input tokens x , layer index ℓ , position p , counterfactual pairs $\{(y_i^0, y_i^1)\}$, step size η , steps T , regularization constant c

Ensure: Steered hidden state h_T

- 1: $h_0 \leftarrow$ hidden state at layer ℓ , position p {standard forward}
- 2: $J_0 \leftarrow Df^{(\ell)}(h_0)$ {Jacobian via d backward passes; computed once}
- 3: **for** $t = 0, 1, \dots, T - 1$ **do**
- 4: **// Covector: gradient of concept probability**
- 5: $q_t \leftarrow \nabla_h P^W(1)|_{h_t}$ {one backward pass through hook forward}
- 6: **// Fisher matrix at current output distribution**
- 7: $\lambda_t \leftarrow f^{(\ell)}(h_t)$ {one forward pass}
- 8: $H_t \leftarrow \nabla^2 A(\lambda_t) = \text{Cov}_{P_{\lambda_t}}(\gamma)$
- 9: **// Pullback Fisher metric (frozen Jacobian)**
- 10: $G_t \leftarrow J_0^\top H_t J_0$
- 11: **// Adaptive Tikhonov regularization**
- 12: $\alpha_t \leftarrow c \cdot \lambda_{\text{med}}(G_t)$ $\{\lambda_{\text{med}}$: median positive eigenvalue}
- 13: **// Fisher-optimal direction (Theorem 3.2)**
- 14: $\delta_t \leftarrow (G_t + \alpha_t I)^{-1} q_t$
- 15: $\delta_t \leftarrow \delta_t / \|\delta_t\|$
- 16: **// Sign correction**
- 17: **if** $P^W(1)|_{h_t + \epsilon \delta_t} < P^W(1)|_{h_t}$ **then**
- 18: $\delta_t \leftarrow -\delta_t$
- 19: **end if**
- 20: $h_{t+1} \leftarrow h_t + \eta \delta_t$
- 21: **end for**
- 22: **return** h_T

All intermediate-layer interventions use a hook-based forward pass: a PyTorch forward hook on the target layer’s output replaces the hidden state at the steering position, and the full model forward pass proceeds normally. This ensures exact correspondence with the unmodified model’s computational path.

Baselines. We compare against four methods:

- **Euclidean gradient ascent:** at each step, move along the normalized gradient $\nabla_h P^W(1) / \|\nabla_h P^W(1)\|$. This uses the same covector as our method but with $G = I$, isolating the effect of the metric.
- **CAA** (Rimsky et al. 2024): the mean activation difference $\mu_+ - \mu_-$ over training contexts. Fixed direction.
- **ActAdd** (Turner et al. 2024): the activation difference from a single contrastive pair. Fixed direction.
- **ITI** (Li et al. 2023): top-6 attention heads selected by probe accuracy, each steered along its per-head probe direction. Fixed direction.

Evaluation protocol. All methods use the same per-context calibrated step size (determined by binary search on the Euclidean gradient direction to reach $P^W = 0.9$ in 30 steps) and the same step budget (30 steps). For each method’s steering path, we apply *exact target crossing bisection*: whenever P^W crosses a target level $\tau \in$

Table 3: Off-target KL comparison at matched concept probability P^W . Ratio = $D_{\text{KL}}^{\text{off}}$ (baseline) / $D_{\text{KL}}^{\text{off}}$ (Ours); values > 1 indicate our method preserves non-target semantics better. Win rate = fraction of cases where our method achieves lower $D_{\text{KL}}^{\text{off}}$.

Baseline	P^W	n	Median	Win %	p
Euclidean	0.3	113	$2.51\times$	81.4	$<10^{-4}$
	0.5	108	$1.91\times$	80.6	$<10^{-4}$
	0.7	102	$1.61\times$	78.4	$<10^{-4}$
	0.9	96	$1.32\times$	<u>72.9</u>	$<10^{-4}$
CAA	0.3	82	$1.58\times$	78.0	$<10^{-4}$
	0.5	76	$1.42\times$	77.6	$<10^{-4}$
	0.7	71	$1.54\times$	76.1	$<10^{-4}$
	0.9	66	$1.50\times$	<u>75.8</u>	$<10^{-4}$
Strongest per-case	0.3	90	$1.65\times$	78.9	$<10^{-4}$
	0.5	83	$1.44\times$	78.3	$<10^{-4}$
	0.7	77	$1.52\times$	74.0	$<10^{-4}$
	0.9	72	$1.50\times$	<u>72.2</u>	1×10^{-4}

{0.3, 0.5, 0.7, 0.9} between consecutive steps, we bisect the $[h_t, h_{t+1}]$ segment to find the point where $P^W = \tau \pm 10^{-3}$, and evaluate all metrics at that exact point. This ensures that comparisons are made at precisely matched concept probabilities.

Results Table 3 reports the main comparison at each target concept probability. Across 300 test cases (3 concepts \times 4 layers \times 25 contexts), 198 pass calibration (66%). Among calibration-successful cases, we compare at each target P^W level using only cases where both methods achieve an exact target crossing.

Our method vs. Euclidean baselines. Our iterative Fisher steering achieves statistically significant improvements over all Euclidean baselines at every target probability level (all $p < 10^{-4}$, one-sided binomial test). At $P^W = 0.3$, the median off-target KL is $2.51\times$ lower than Euclidean gradient ascent; at the most demanding target $P^W = 0.9$, our method maintains a $1.32\times$ advantage with a 72.9% win rate ($n = 96$). The ‘‘Strongest per-case’’ row compares against the baseline with the lowest $D_{\text{KL}}^{\text{off}}$ among CAA, ActAdd, and ITI for each individual case—the most favorable comparison possible for the baselines. Even against this oracle-selected competitor, our method achieves a median advantage of $1.50\times$ at $P^W = 0.9$ with 72.2% win rate, indicating that the benefit of Fisher metric correction is not confined to weak baselines. The advantage varies across concepts: `verb_third` shows the strongest improvement (93.9% win rate at $P^W = 0.9$, median $1.82\times$), while `verb_past` shows a more modest effect (median $1.16\times$), consistent with the greater heterogeneity of irregular verb forms in the latter concept’s unembedding geometry. A per-concept breakdown is provided in Appendix D.

Steering efficiency. Because the Fisher-optimal direction allocates its perturbation budget to minimize output distortion rather than maximize concept change, it achieves less concept change per step than the Euclidean direction.

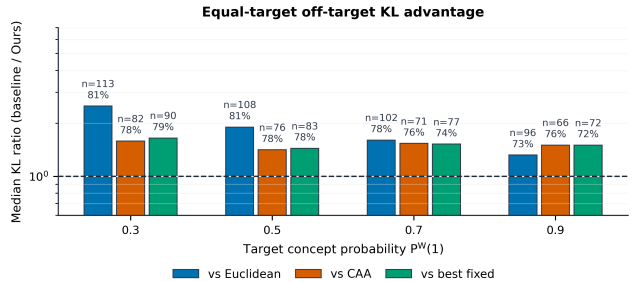


Figure 3: Median off-target KL ratio (baseline / Ours) at four target concept probabilities, aggregated over all concepts and layers. Values above the dashed line (= 1) indicate our method achieves lower off-target KL. Sample sizes and win rates are annotated above each bar. Our method consistently outperforms all baselines, with the advantage most pronounced at lower target probabilities where geometric correction has the greatest effect.

Table 4: Target crossing coverage: fraction of calibration-successful cases ($n = 198$) where each method reaches the indicated P^W within 30 steps. The step size is calibrated for the Euclidean direction; other methods inherit this step size.

Method	$P^W=0.3$	$P^W=0.5$	$P^W=0.7$	$P^W=0.9$
Euclidean	100%	100%	100%	100%
CAA	52%	46%	41%	36%
ITI	30%	29%	28%	23%
ActAdd	14%	11%	10%	8%
Ours (Fisher iter.)	57%	55%	52%	48%

Table 4 reports the fraction of cases where each method reaches each target P^W within the fixed step budget. Note that the step size is calibrated for the Euclidean direction; all other methods inherit this step size.

Euclidean gradient ascent achieves 100% coverage by construction (the step size is calibrated for this direction). Our method’s coverage (48–57%) is comparable to or higher than that of CAA (36–52%), and substantially exceeds ITI and ActAdd. This pattern reflects a precision-efficiency trade-off intrinsic to geometry-aware methods: by directing perturbation energy away from high-Fisher-curvature directions, the Fisher-optimal direction preserves off-target semantics at the cost of slower concept change. The effect is layer-dependent: at intermediate depths (Layers 3, 6, 9), our method reaches high target probabilities in a substantial fraction of cases, while at the deepest layer (Layer 11), the Fisher direction diverges most from the Euclidean gradient—as expected from the theory, since the pullback metric is closest to the output Fisher at this depth—and coverage decreases. Independently calibrating the step size for the Fisher direction or increasing the step budget would improve coverage; we leave this to future work.

We note that the comparisons in Table 3 condition on both methods reaching the target, which is the appropriate comparison for our theoretical claim: Theorem 3.2 asserts

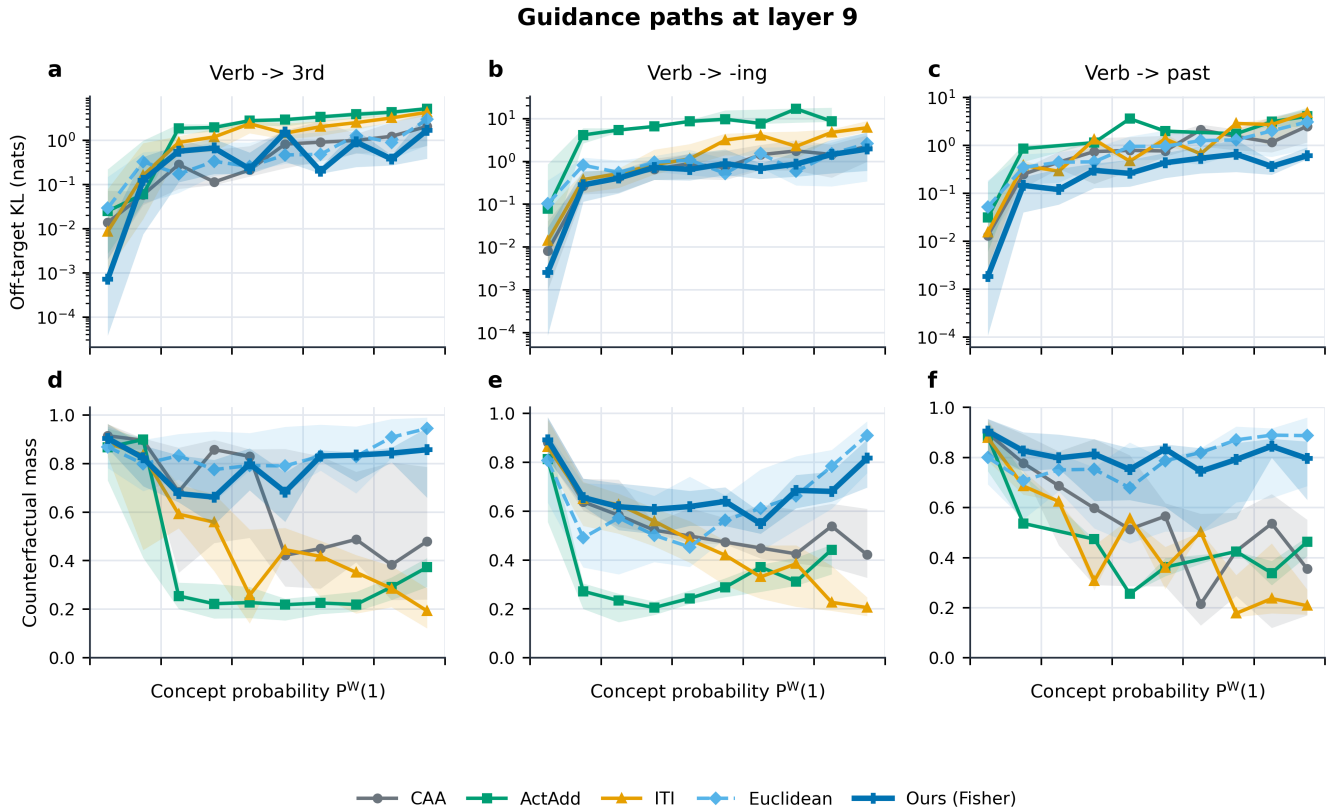


Figure 4: Steering paths at Layer 9 across three verb-morphology concepts. **Top row (a–c):** Off-target KL divergence $D_{\text{KL}}^{\text{off}}$ (log scale) as a function of concept probability $P^W(1)$. Our method (dark blue, solid) achieves consistently lower off-target KL than Euclidean gradient ascent (light blue, dashed) and all fixed-direction baselines at matched concept probability. **Bottom row (d–f):** Counterfactual mass preservation. Our method retains more probability mass on concept-relevant tokens throughout the steering path. Lines show medians; shaded regions show interquartile ranges. Additional layers are shown in Appendix D.

that the Fisher direction minimizes $D_{\text{KL}}^{\text{off}}$ at a given concept change level, not that it reaches that level with fewer steps. Tables 3 and 4 together give a complete picture: the former quantifies the precision advantage, the latter quantifies the efficiency trade-off.

6 Related Work

Activation steering. Modifying intermediate representations to control model behavior dates to the Plug-and-Play Language Model (Dathathri et al. 2020), which uses a separate classifier to perturb activations toward a target attribute. Modern steering methods bypass the classifier: Turner et al. (2024) show that a single direction vector, extracted from contrastive prompt pairs and added to a residual stream activation, can shift high-level properties such as sentiment and topic. Rimsky et al. (2024) scale this to hundreds of contrastive examples (CAA), and Li et al. (2023) select per-head steering directions via linear probes (ITI). Subsequent work has explored covariance-weighted directions (Singh et al. 2024), trained low-rank interventions (Wu et al. 2025), concept erasure via optimal affine projections (Belrose et al. 2023), safety-oriented refusal steering (Arditi et al. 2024),

and depth-adaptive coefficient schedules (van der Weij, Poesio, and Schoots 2024; Vu and Nguyen 2025). Im and Li (2025) provide a unified comparison of direction-selection strategies within the Euclidean framework. Despite their diversity, all of these methods share a common implicit assumption: the activation space is Euclidean, and the natural intervention is additive ($h' = h + \alpha v$). Our work removes this assumption by deriving the correct non-Euclidean metric from the model’s own computational structure.

Information geometry of neural networks. The Fisher information matrix has a long history as the natural Riemannian metric on statistical model manifolds (Rao 1945; Amari 1998, 2016). In deep learning, its role is best known through natural gradient descent, which preconditions parameter updates by the inverse Fisher to achieve parameterization-invariant optimization (Amari 1998; Martens 2020). Practical approximations such as K-FAC exploit the Kronecker structure of layer-wise Fisher blocks to make natural gradient tractable at scale. The connection between the Fisher metric and the KL divergence—specifically, that $D_{\text{KL}} \approx \frac{1}{2} \Delta\theta^\top F \Delta\theta$ to second order—is the mathematical foundation of our pullback construction.

However, prior work on natural gradient operates in *parameter* space, whereas we apply the Fisher metric in *activation* space: rather than preconditioning weight updates during training, we precondition activation perturbations during inference-time steering.

Riemannian geometry of latent representations.

Pullback Riemannian metrics have been studied extensively in the context of generative models. Arvanitidis, Hansen, and Hauberg (2018) show that pulling back the Euclidean data-space metric through a VAE decoder reveals the latent space’s intrinsic geometry, enabling geometrically meaningful interpolation along geodesics rather than straight lines. Arvanitidis et al. (2022) extend this to pulling back the Fisher information metric itself, connecting latent geometry to probabilistic structure. These ideas have been applied to curvature estimation, improved sampling, and representation alignment. Our construction follows the same mathematical principle—pulling back a target-space metric through a smooth map’s Jacobian—but applies it to a fundamentally different setting: the residual stream of a frozen Transformer at inference time, with the softmax Fisher as the target-space metric and activation steering as the application.

Geometry-aware steering. Three concurrent works address the geometry of activation steering. Park et al. (2026) rigorously characterize the output-layer Fisher–Rao geometry of the softmax distribution, proving that dual-coordinate steering optimally preserves off-target semantics. Their theory applies to the final representation layer; our work extends the Fisher geometry to arbitrary intermediate layers via the Jacobian pullback. Wurgaft et al. (2026) empirically discover that intermediate activation manifolds exhibit significant non-Euclidean structure and propose data-driven manifold steering based on spline fitting and pullback optimization. Raval et al. (2026) use VAE ensembles with pullback Riemannian metrics and kernel PCA to construct non-linear steering directions. Both of these latter approaches identify the same qualitative phenomenon—intermediate-layer geometry is non-Euclidean—but rely on data-driven estimation without formal characterization of the geometry or optimality guarantees for the resulting directions. Our work complements these approaches by providing an *analytical* derivation of the intermediate-layer metric, a closed-form optimal steering equation, and a unified framework that explains existing methods as special cases.

7 Conclusion

This paper establishes the information-geometric foundation for activation steering at intermediate Transformer layers. We derive the pullback Fisher metric $G^{(\ell)} = J^T H J$ —the unique Riemannian metric that captures how perturbations at layer ℓ affect the output distribution—and prove a closed-form optimal steering equation that minimizes off-target KL divergence at any prescribed concept change level. The metric’s layer-wise recursive structure $G^{(\ell)} = A_\ell^T G^{(\ell+1)} A_\ell$ yields explicit depth bounds on the condition number and provides the first formal explanation for why steering effectiveness varies across layers. Through a uni-

fied information-geometric framework, we show that existing Euclidean steering methods—CAA, ActAdd, ITI, and others—each implicitly operate under a specific approximate metric, and that their performance gaps are quantitatively predicted by the Fisher–Pythagorean excess cost decomposition.

Empirically, we confirm on GPT-2 that the pullback Fisher metric deviates from the Euclidean metric by over 97% in relative spectral norm, with condition numbers exceeding 10^7 . Iterative Fisher steering, which applies the optimal equation with updated covectors and Fisher matrices at each step, reduces off-target KL by $1.3\times$ – $2.5\times$ relative to Euclidean gradient steering and $1.5\times$ relative to CAA at matched concept probability, with win rates of 72–81% ($p < 10^{-4}$).

Limitations. Our experimental validation is conducted on GPT-2 small (124M parameters). While the theoretical framework applies to any decoder-only Transformer with a softmax output layer, the empirical conclusions—particularly the magnitude of the Fisher advantage and the behavior of the frozen Jacobian approximation—may differ at larger scales where the residual stream geometry and spectral structure of the pullback metric could exhibit qualitatively different patterns. Additionally, the current iterative procedure uses a step size calibrated for the Euclidean direction, which leads to reduced coverage for the Fisher direction at certain layers. Independent step-size calibration or adaptive step budgets would likely improve coverage but require additional computational investment.

Future work. Several directions naturally extend this work. First, scaling experiments to 8B-parameter models (Llama-3, Gemma-2) using randomized approximations of the pullback metric will test whether the Fisher advantage persists—and potentially strengthens—at scale, where the depth and width of the residual stream may amplify geometric anisotropy. Second, the framework extends in principle to any model whose output head is a softmax over discrete tokens; applying it to vision-language-action models for robotic control, where steering intermediate representations could enable precise behavioral adjustments without retraining, is a promising application domain. Third, extending the concept vocabulary beyond verb morphology to semantic concepts (sentiment, truthfulness, safety compliance) will test the generality of the geometric advantage. Finally, developing more efficient Jacobian approximations—such as low-rank updates or amortized estimation across contexts—would reduce the per-context computational overhead and make Fisher steering practical for real-time applications.

References

Amari, S.-i. 1998. Natural Gradient Works Efficiently in Learning. *Neural Computation*, 10(2): 251–276.

Amari, S.-i. 2016. *Information Geometry and Its Applications*. Springer.

Arditi, A.; Obeso, O.; Syed, A.; Paleka, D.; Panickssery, N.; Gurnee, W.; and Nanda, N. 2024. Refusal in Language Models Is Mediated by a Single Direction. *arXiv preprint arXiv:2406.11717*.

- Arvanitidis, G.; González-Duque, M.; Pouplin, A.; Kalatzis, D.; and Hauberg, S. 2022. Pulling Back Information Geometry. In *International Conference on Artificial Intelligence and Statistics*.
- Arvanitidis, G.; Hansen, L. K.; and Hauberg, S. 2018. Latent Space Oddity: On the Curvature of Deep Generative Models. In *International Conference on Learning Representations*.
- Ba, J. L.; Kiros, J. R.; and Hinton, G. E. 2016. Layer Normalization. *arXiv preprint arXiv:1607.06450*.
- Banerjee, A.; Merugu, S.; Dhillon, I. S.; and Ghosh, J. 2005. Clustering with Bregman Divergences. *Journal of Machine Learning Research*, 6: 1705–1749.
- Belrose, N.; Schneider-Joseph, D.; Ravfogel, S.; Cotterell, R.; Raff, E.; and Biderman, S. 2023. LEACE: Perfect linear concept erasure in closed form. In *Thirty-seventh Conference on Neural Information Processing Systems*.
- Dathathri, S.; Madotto, A.; Lan, J.; Hung, J.; Frank, E.; Molino, P.; Yosinski, J.; and Liu, R. 2020. Plug and Play Language Models: A Simple Approach to Controlled Text Generation. *arXiv preprint arXiv:1912.02164*.
- Im, J.; and Li, J. 2025. A Unified Framework for Understanding Activation Steering Directions. *arXiv preprint arXiv:2502.02716*.
- Li, K.; Patel, O.; Viégas, F.; Pfister, H.; and Wattenberg, M. 2023. Inference-Time Intervention: Eliciting Truthful Answers from a Language Model. In *Advances in Neural Information Processing Systems*, volume 36.
- Martens, J. 2020. New Insights and Perspectives on the Natural Gradient Method. *Journal of Machine Learning Research*, 21(146): 1–76.
- Park, K.; Nief, T.; Choe, Y. J.; and Veitch, V. 2026. The Information Geometry of Softmax: Probing and Steering. *arXiv preprint arXiv:2602.15293*.
- Radford, A.; Wu, J.; Child, R.; Luan, D.; Amodei, D.; and Sutskever, I. 2019. Language Models are Unsupervised Multitask Learners. *OpenAI Blog*.
- Raffel, C.; Shazeer, N.; Roberts, A.; Lee, K.; Narang, S.; Matena, M.; Zhou, Y.; Li, W.; and Liu, P. J. 2020. Exploring the Limits of Transfer Learning with a Unified Text-to-Text Transformer. *Journal of Machine Learning Research*, 21(140): 1–67.
- Rao, C. R. 1945. Information and the Accuracy Attainable in the Estimation of Statistical Parameters. *Bulletin of the Calcutta Mathematical Society*, 37: 81–91.
- Raval, S.; Song, H. J.; Wu, L.; Harrasse, A.; Phillips, J. M.; Barez, F.; and Abdullah, A. 2026. Curveball Steering: The Right Direction To Steer Isn’t Always Linear. *arXiv preprint arXiv:2603.09313*.
- Rimsky, N.; Gabrieli, N.; Schulz, J.; Tong, M.; Hubinger, E.; and Turner, A. 2024. Steering Llama 2 via Contrastive Activation Addition. In *Proceedings of the 62nd Annual Meeting of the Association for Computational Linguistics (Volume 1: Long Papers)*, 15504–15522. Association for Computational Linguistics.
- Singh, S.; Ravfogel, S.; Herzig, J.; Aharoni, R.; Cotterell, R.; and Kumaraguru, P. 2024. Representation Surgery: Theory and Practice of Affine Steering. In *Proceedings of the 41st International Conference on Machine Learning*.
- Turner, A. M.; Thiergart, L.; Leech, G.; Udell, D.; Vazquez, J. J.; Mini, U.; and MacDiarmid, M. 2024. Steering Language Models With Activation Engineering. *arXiv preprint arXiv:2308.10248*.
- van der Weij, T.; Poesio, M.; and Schoots, N. 2024. Extending Activation Steering to Broad Skills and Multiple Behaviours. *arXiv preprint arXiv:2403.05767*.
- Vu, H. M.; and Nguyen, T. M. 2025. Angular Steering: Behavior Control via Rotation in Activation Space. In *2nd Workshop on Models of Human Feedback for AI Alignment*.
- Wu, Z.; Arora, A.; Geiger, A.; Huang, J.; Wang, Z.; Manning, C. D.; and Potts, C. 2025. AxBench: Steering LLMs? Benchmark and Decompose the Steering Ability of Representation Intervention Methods. In *Proceedings of the 42nd International Conference on Machine Learning*.
- Wurgaft, D.; et al. 2026. Manifold Steering: Turning, Not Transplanting, Activations for Controllable Generation. *arXiv preprint arXiv:2605.05115*.
- Zou, A.; Phan, L.; Chen, S.; Campbell, J.; Guo, P.; Ren, R.; Pan, A.; Yin, X.; Mazeika, M.; Dombrowski, A.-K.; et al. 2023. Representation Engineering: A Top-Down Approach to AI Transparency. *arXiv preprint arXiv:2310.01405*.

Appendix

A Proofs for Global Optimality (Proposition 3.7)

Proof of Proposition 3.7. Let $T = \text{Im}(A)$ denote the reachable output tangent space, and $T_c = T \cap \ker(\beta_W^\top)$ the feasible tangent space. The objective is

$$F(\lambda) = D_{\text{KL}}(P_{\lambda_0} \| P_\lambda) = A(\lambda) - A(\lambda_0) - \phi(\lambda_0)^\top (\lambda - \lambda_0),$$

with gradient $\nabla_\lambda F = \phi(\lambda) - \phi(\lambda_0)$. Since A is strictly convex, F is strictly convex, and the minimizer $\hat{\lambda}$ over the closed convex feasible set is unique. At $\hat{\lambda}$, the gradient must lie in T_c^\perp :

$$\phi(\hat{\lambda}) - \phi(\lambda_0) \in T_c^\perp = (T \cap \ker \beta_W^\top)^\perp = T^\perp + \text{span}\{\beta_W\}.$$

So there exist $\xi \in T^\perp$ and $\nu \in \mathbb{R}$ with

$$\phi(\hat{\lambda}) - \phi(\lambda_0) + \nu \beta_W + \xi = 0.$$

Left-multiplying by A^\top annihilates ξ (since $A^\top \xi = 0$ for $\xi \perp \text{Im}(A)$):

$$A^\top (\phi(\hat{\lambda}) - \phi(\lambda_0)) + \nu q = 0,$$

where $q = A^\top \beta_W$. □

First-order expansion of the global solution. The KKT condition in h -coordinates reads

$$A^\top (\phi(\lambda_0 + A \delta h) - \phi(\lambda_0)) + \nu q = 0.$$

Taylor-expanding ϕ :

$$\phi(\lambda_0 + A \delta h) - \phi(\lambda_0) = H(\lambda_0) A \delta h + O(\|\delta h\|^2).$$

Substituting and defining $G_0 = A^\top H(\lambda_0) A$:

$$G_0 \delta h + \nu q + O(\|\delta h\|^2) = 0.$$

The leading-order system is $G_0 \delta h + \nu q = 0$, $q^\top \delta h = \rho$. Its minimum-norm solution is $\delta h = -\nu G_0^+ q$ with $\nu = -\rho / (q^\top G_0^+ q)$. By the implicit function theorem applied to the full nonlinear KKT system:

$$\delta h^*(\rho) = \frac{\rho}{q^\top G_0^+ q} G_0^+ q + O(\rho^2). \quad \square$$

Critical step size. The second-order KL approximation has remainder $|R_3| \leq C_3 \|\delta h\|^3$. It is accurate to relative error ϵ when $\|\delta h\| \leq r_{\text{crit}} := \epsilon \lambda_{\min}^+(G) / C_3$. On our toy models, $r_{\text{crit}} \in [3 \times 10^{-4}, 3 \times 10^{-3}]$, yet the direction remains accurate ($\cos > 0.997$) at 80–1000× larger step sizes (Figure 1). This gap is explained by Theorem 3.8 (Appendix B).

B Proof of Direction Stability (Theorem 3.8)

Proof. The true local optimization problem is

$$\min_{\delta} D_{\text{KL}}(P_{f(h_0)} \| P_{f(h_0+\delta)}) \quad \text{s.t.} \quad \beta_W^\top f(h_0+\delta) - \beta_W^\top f(h_0) = \rho.$$

Expanding around $\delta = 0$:

$$\text{Objective:} \quad \frac{1}{2} \delta^\top G_0 \delta + O(\|\delta\|^3),$$

$$\text{Constraint:} \quad q_0^\top \delta + O(\|\delta\|^2) = \rho.$$

The KKT conditions for the nonlinear problem are

$$G_0 \delta + \nu q_0 + R_1(\delta, \nu) = 0, \quad (33)$$

$$q_0^\top \delta + R_2(\delta) = \rho, \quad (34)$$

where $\|R_1\| = O(\|\delta\|^2 + |\nu| \|\delta\|)$ and $|R_2| = O(\|\delta\|^2)$. The linearized system (setting $R_1 = R_2 = 0$) has the solution

$$\delta_0(\rho) = \frac{\rho}{q_0^\top G_0^+ q_0} G_0^+ q_0.$$

The Jacobian of the KKT mapping at (δ_0, ν_0) is

$$\begin{bmatrix} G_0 & q_0 \\ q_0^\top & 0 \end{bmatrix},$$

which is nonsingular on $\text{Range}(G_0) \times \mathbb{R}$ when $q_0^\top G_0^+ q_0 > 0$. By the implicit function theorem, there exists a C^1 solution curve with

$$\delta_*(\rho) = \delta_0(\rho) + e(\rho), \quad \|e(\rho)\| = O(\rho^2).$$

For the cosine bound, let $u_0 = \delta_0 / \|\delta_0\|$ and $u_* = \delta_* / \|\delta_*\|$. Since $\|\delta_0\| = \Theta(\rho)$ and $\|e\| = O(\rho^2)$:

$$\|u_* - u_0\| = O\left(\frac{\|e\|}{\|\delta_0\|}\right) = O(\rho).$$

Using $1 - u_*^\top u_0 = \frac{1}{2} \|u_* - u_0\|^2$:

$$1 - \cos(\delta_*, \delta_0) = O(\rho^2). \quad \square$$

C Proof of Non-target KL Optimality (Theorem 3.11)

Proof. Under concept decomposability, the total KL decomposes. For counterfactual pairs:

$$\begin{aligned} & \sum_{i,w} P_{\lambda_0}(y_i^w) \log \frac{P_{\lambda_0}(y_i^w)}{P_\lambda(y_i^w)} \\ &= \sum_i P_{\lambda_0}^Z(z_i) \sum_w P_{\lambda_0}^W(w) \log \frac{P_{\lambda_0}^W(w)}{P_\lambda^W(w)} \\ & \quad + \sum_i P_{\lambda_0}^Z(z_i) \log \frac{P_{\lambda_0}^Z(z_i)}{P_\lambda^Z(z_i)}. \end{aligned}$$

Adding the neutral tokens $y \notin \mathcal{Y}_W$:

$$\begin{aligned} D_{\text{KL}}(P_{\lambda_0} \| P_\lambda) &= \left(\sum_i P_{\lambda_0}^Z(z_i) \right) D_{\text{KL}}(P_{\lambda_0}^W \| P_\lambda^W) \\ & \quad + D_{\text{KL}}(P_{\lambda_0}^Z \| P_\lambda^Z). \end{aligned} \quad (35)$$

On \mathcal{A}_c , $\beta_W^\top f(h) = c$ is fixed, so $P_\lambda^W(1) = \sigma(c + b_W) = \text{const}$. The first term in (35) is constant, so minimizing total KL is equivalent to minimizing $D_{\text{KL}}(P_{\lambda_0}^Z \| P_\lambda^Z)$.

For the second-order extension: $\delta h^\top G \delta h$ approximates the total KL. Under decomposability, this quadratic form inherits the decomposition to second order. On the linearized constraint $q^\top \delta h = \rho$, the concept KL contribution is fixed, so minimizing $\delta h^\top G \delta h$ simultaneously minimizes the second-order off-target KL. □

D Additional Experimental Results

D.1 Per-concept Breakdown

Table 5: Per-concept comparison: Ours vs. Euclidean at $P^W = 0.9$.

Concept	n	Median	Win %	p
verb_third	33	1.82×	93.9	$<10^{-4}$
verb_ing	41	1.24×	63.4	0.063
verb_past	22	1.16×	59.1	0.262

The advantage is strongest for `verb_third`, which consists primarily of regular morphological inflections with consistent unembedding geometry. The more modest effect on `verb_past` is consistent with the greater heterogeneity of irregular verb forms, whose unembedding difference vectors point in diverse directions.

D.2 Per-layer Steering Paths

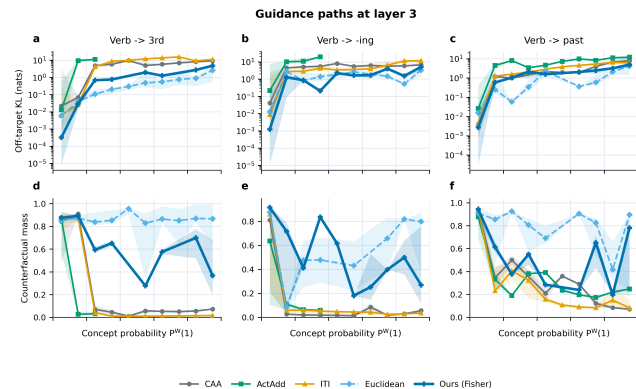


Figure 5: Steering paths at Layer 3. Our method (dark blue) achieves substantially lower off-target KL than all baselines across all three concepts. Counterfactual mass preservation is also higher.

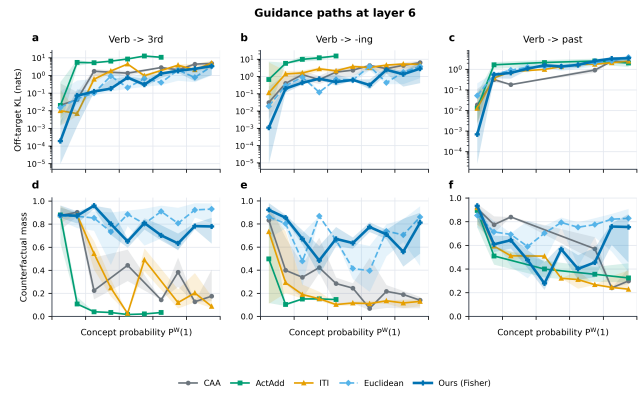


Figure 6: Steering paths at Layer 6. The pattern is consistent with Layer 3: our method maintains lower off-target KL throughout the steering path.

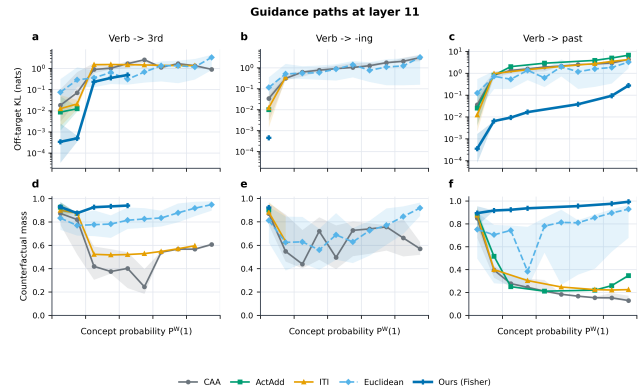


Figure 7: Steering paths at Layer 11. Our method achieves low off-target KL and high counterfactual mass in the available concept probability range.

D.3 Layer-wise Advantage

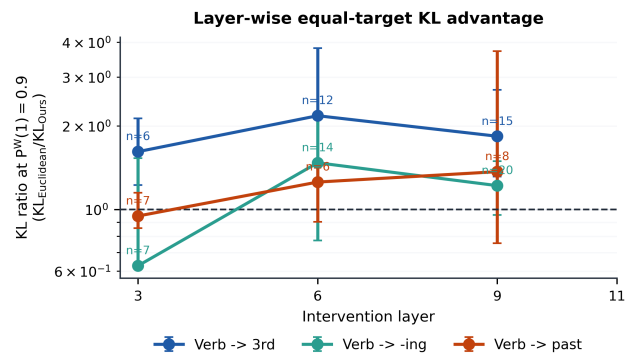


Figure 8: Layer-wise off-target KL ratio (Euclidean / Ours) at $P^W(1) = 0.9$, by concept. Points above the dashed line indicate our method achieves lower off-target KL. Error bars show interquartile ranges.

E Spectral Analysis

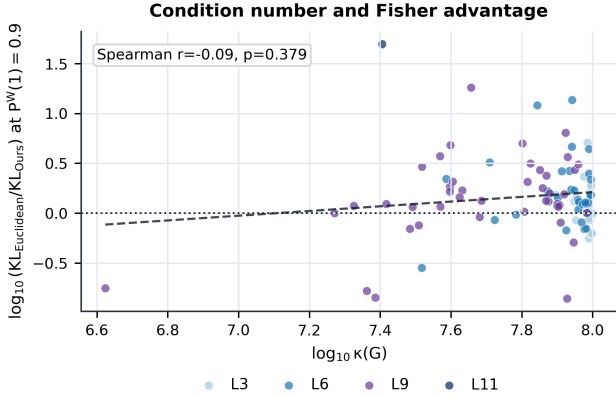


Figure 9: Condition number $\kappa(G)$ vs. off-target KL ratio at $P^W(1) = 0.9$. The Spearman correlation is not significant ($r = -0.09$, $p = 0.38$), likely due to insufficient dynamic range: all condition numbers fall within $10^{6.5-10^8}$.

F Deferred Proofs from Section 3

F.1 Characterization of Concept Decomposability (Lemma 3.10)

Proof. Decomposability requires $P_\lambda(y_i^1)/P_\lambda(y_i^0)$ to be independent of i . By the softmax form:

$$\frac{P_\lambda(y_i^1)}{P_\lambda(y_i^0)} = \exp(d_i^\top \lambda), \quad d_i = \gamma_{y_i^1} - \gamma_{y_i^0}.$$

This is i -independent iff $d_i^\top \lambda = d_j^\top \lambda$ for all i, j . \square

F.2 GGN Equivalence

Proposition F.1 (Pullback Fisher = GGN). *For softmax with cross-entropy loss $\mathcal{L}_y(\lambda) = -\log P_\lambda(y)$:*

$$\nabla_\lambda^2 \mathcal{L}_y(\lambda) = \nabla_\lambda^2 A(\lambda) = H(\lambda),$$

independent of label y . Therefore the generalized Gauss–Newton matrix at intermediate layer ℓ is

$$G_{\text{GGN}} = J^\top H J = G^{(\ell)}.$$

Proof. The cross-entropy loss is $\mathcal{L}_y = A(\lambda) - \gamma_y^\top \lambda$. The second term is linear, so $\nabla_\lambda^2 \mathcal{L}_y = \nabla_\lambda^2 A = H$. The GGN of \mathcal{L}_y with respect to h through the map $\lambda = f(h)$ is $J^\top (\nabla_\lambda^2 \mathcal{L}_y) J = J^\top H J$. \square

This connects activation steering to the natural gradient literature (Amari 1998; Martens 2020): Fisher steering at layer ℓ is equivalent to a single natural gradient step on the per-sample loss, treating h as a virtual parameter.

F.3 Scale Equivariance (Theorem 3.12)

Proof. Let $\alpha(G) = c \cdot \lambda_{\text{med}}(G)$. If $\tilde{G} = sG$, then $\lambda_{\text{med}}(\tilde{G}) = s \lambda_{\text{med}}(G)$, so $\alpha(\tilde{G}) = s \alpha(G)$ and

$$\tilde{G} + \alpha(\tilde{G}) I = sG + s\alpha(G) I = s(G + \alpha(G) I).$$

Inverting: $(\tilde{G} + \alpha(\tilde{G}) I)^{-1} q = \frac{1}{s} (G + \alpha(G) I)^{-1} q$. The factor $1/s$ cancels under normalization. \square

E.4 Tikhonov Bias Bound (Theorem 3.13)

Proof. In the eigenbasis of G with eigenvalues $\lambda_i > 0$, the i -th component of the difference is

$$\begin{aligned} (\delta_\alpha - G^+ q)_i &= \frac{q_i}{\lambda_i + \alpha} - \frac{q_i}{\lambda_i} \\ &= -\frac{\alpha}{\lambda_i(\lambda_i + \alpha)} q_i = -\frac{\alpha}{\lambda_i + \alpha} (G^+ q)_i. \end{aligned}$$

Since $\alpha/(\lambda_i + \alpha) \leq \alpha/(\lambda_r + \alpha)$ for all $\lambda_i \geq \lambda_r$, the bound follows. \square

G Unified Framework: Proofs from Section 4

This appendix provides complete proofs for the unified information-geometric framework of Section 4.

G.1 Fisher–Pythagorean Excess Cost Identity

Theorem G.1 (Fisher–Pythagorean identity). *Let $G \succ 0$ and δ_G^* be the Fisher-optimal direction (Theorem 3.2). For any $\tilde{\delta}$ satisfying $q^\top \tilde{\delta} = \rho$:*

$$C_G(\tilde{\delta}) - C_G(\delta_G^*) = \frac{1}{2} (\tilde{\delta} - \delta_G^*)^\top G (\tilde{\delta} - \delta_G^*). \quad (36)$$

Proof. Let $e = \tilde{\delta} - \delta_G^*$. Since both satisfy $q^\top \tilde{\delta} = \rho$, we have $q^\top e = 0$. By the KKT condition, $G \delta_G^* = \nu q$ for some scalar ν , so $e^\top G \delta_G^* = \nu e^\top q = 0$. Expanding:

$$\begin{aligned} C_G(\tilde{\delta}) &= \frac{1}{2} (\delta_G^* + e)^\top G (\delta_G^* + e) \\ &= \frac{1}{2} \delta_G^{*\top} G \delta_G^* + \underbrace{e^\top G \delta_G^*}_{=0} + \frac{1}{2} e^\top G e \\ &= C_G(\delta_G^*) + \frac{1}{2} e^\top G e. \end{aligned} \quad \square$$

G.2 Spectral Decomposition of Excess Cost

Theorem G.2 (Spectral excess cost). *Let $G = \sum_i \lambda_i u_i u_i^\top$ with $\lambda_i > 0$, and let $e_i = u_i^\top (\tilde{\delta} - \delta_G^*)$. Then*

$$\Delta C_G(\tilde{\delta}) = \frac{1}{2} \sum_{i=1}^d \lambda_i e_i^2.$$

Proof. Direct substitution of G 's spectral decomposition into (36):

$$e^\top G e = e^\top \left(\sum_i \lambda_i u_i u_i^\top \right) e = \sum_i \lambda_i (u_i^\top e)^2. \quad \square$$

Corollary G.3 (Low-curvature error tolerance). *If $u_i^\top e = 0$ for $i = 1, \dots, k$ (error is absent in the top- k Fisher directions), then $\Delta C_G(\tilde{\delta}) \leq \frac{1}{2} \lambda_{k+1} \|e\|^2$.*

G.3 Proxy Metric Cost Formula

Theorem G.4 (Cost of proxy metric steering). *If a method uses proxy metric $M \succ 0$ with direction $\delta_M = \rho M^{-1} q / (q^\top M^{-1} q)$, its true Fisher cost is*

$$C_G(\delta_M) = \frac{\rho^2 q^\top M^{-1} G M^{-1} q}{2 (q^\top M^{-1} q)^2},$$

and the cost ratio relative to Fisher-optimal is

$$R_G(M; q) = \frac{C_G(\delta_M)}{C_G(\delta_G^*)} = \frac{q^\top M^{-1} G M^{-1} q}{(q^\top M^{-1} q)^2} \cdot (q^\top G^{-1} q) \geq 1. \quad (37)$$

Proof. Direct computation:

$$\begin{aligned} C_G(\delta_M) &= \frac{1}{2} \delta_M^\top G \delta_M \\ &= \frac{\rho^2}{2} \frac{(M^{-1}q)^\top G (M^{-1}q)}{(q^\top M^{-1}q)^2} \\ &= \frac{\rho^2}{2} \frac{q^\top M^{-1} G M^{-1} q}{(q^\top M^{-1} q)^2}. \end{aligned}$$

Dividing by $C_G(\delta_G^*) = \rho^2 / (2q^\top G^{-1}q)$ gives the ratio. The inequality $R_G \geq 1$ follows from the optimality of δ_G^* . \square

G.4 Whitened Form and Weighted Variance Interpretation

Theorem G.5 (Whitened cost ratio). *Define $\nu = G^{-1/2}q / \sqrt{q^\top G^{-1}q}$ (unit vector) and $B = G^{1/2}M^{-1}G^{1/2}$. Then*

$$R_G(M; q) = \frac{\nu^\top B^2 \nu}{(\nu^\top B \nu)^2}.$$

If B has spectral decomposition $B = \sum_i b_i r_i r_i^\top$ and $w_i = (r_i^\top \nu)^2$, then

$$R_G(M; q) = \frac{\sum_i w_i b_i^2}{(\sum_i w_i b_i)^2} = 1 + \frac{\text{Var}_w(b)}{(\mathbb{E}_w[b])^2}. \quad (38)$$

Proof. Substituting $q = G^{1/2}\nu\sqrt{q^\top G^{-1}q}$ into (37):

$$\begin{aligned} q^\top M^{-1}q &= (q^\top G^{-1}q) \nu^\top B \nu, \\ q^\top M^{-1}G M^{-1}q &= (q^\top G^{-1}q) \nu^\top B^2 \nu. \end{aligned}$$

The ratio simplifies to $\nu^\top B^2 \nu / (\nu^\top B \nu)^2$. Expanding in the eigenbasis of B gives (38). \square

The interpretation: $R_G(M; q)$ equals 1 plus the squared coefficient of variation of B 's eigenvalues, weighted by the direction ν . If B is nearly scalar in the direction ν , then $R_G \approx 1$ regardless of how far M is from G in other directions.

G.5 Kantorovich Bound

Theorem G.6 (Kantorovich bound on cost ratio). *If $\|G^{-1/2}(M - G)G^{-1/2}\|_2 \leq \eta < 1$, then*

$$R_G(M; q) \leq \frac{1}{1 - \eta^2}$$

for all unit vectors q , and

$$C_G(\delta_M) - C_G(\delta_G^*) \leq C_G(\delta_G^*) \frac{\eta^2}{1 - \eta^2}.$$

Proof. Let $S = G^{-1/2}(M - G)G^{-1/2}$ with $\|S\|_2 \leq \eta$. Then $M = G^{1/2}(I + S)G^{1/2}$ and $B = (I + S)^{-1}$ has eigenvalues in $[1/(1 + \eta), 1/(1 - \eta)]$. By the Kantorovich inequality, for any unit vector ν :

$$\frac{\nu^\top B^2 \nu}{(\nu^\top B \nu)^2} \leq \frac{(a + b)^2}{4ab}$$

with $a = 1/(1 + \eta)$ and $b = 1/(1 - \eta)$. Computing:

$$\frac{(a + b)^2}{4ab} = \frac{\left(\frac{1}{1 + \eta} + \frac{1}{1 - \eta}\right)^2}{4 \cdot \frac{1}{1 + \eta} \cdot \frac{1}{1 - \eta}} = \frac{1}{1 - \eta^2}. \quad \square$$

G.6 Implicit Metric of CAA

Theorem G.7 (CAA uses Σ^{-1} as proxy metric). *Under a shared-covariance Gaussian model $h \mid W=w \sim \mathcal{N}(\mu_w, \Sigma)$, the Bayes-optimal log-odds probe is $q_{\text{LDA}} = \Sigma^{-1}(\mu_+ - \mu_-)$. The CAA direction $v_{\text{CAA}} = \mu_+ - \mu_-$ satisfies*

$$v_{\text{CAA}} = \Sigma q_{\text{LDA}},$$

so CAA is equivalent to steering with proxy metric $M_{\text{CAA}} = \Sigma^{-1}$.

Proof. The log-odds is

$$\begin{aligned} \log \frac{p_+(h)}{p_-(h)} &= -\frac{1}{2}(h - \mu_+)^\top \Sigma^{-1}(h - \mu_+) \\ &\quad + \frac{1}{2}(h - \mu_-)^\top \Sigma^{-1}(h - \mu_-) \\ &= (\mu_+ - \mu_-)^\top \Sigma^{-1} h + \text{const.} \end{aligned}$$

So $q_{\text{LDA}} = \Sigma^{-1}(\mu_+ - \mu_-)$ and $v_{\text{CAA}} = \mu_+ - \mu_- = \Sigma q_{\text{LDA}}$, which means $\Sigma^{-1} v_{\text{CAA}} = q$, i.e., $M_{\text{CAA}}^{-1} q = v_{\text{CAA}}$ with $M_{\text{CAA}} = \Sigma^{-1}$. \square

G.7 ITI Subspace Decomposition

Theorem G.8 (ITI excess cost decomposition). *Let $S \subset \{1, \dots, n_{\text{heads}}\}$ be the selected head set and V_S the corresponding subspace projector. The ITI direction δ_{ITI} satisfies*

$$\begin{aligned} C_G(\delta_{\text{ITI}}) - C_G(\delta_G^*) &= \underbrace{C_G(\delta_S^*) - C_G(\delta_G^*)}_{\text{subspace missing cost}} \\ &\quad + \underbrace{C_G(\delta_{\text{ITI}}) - C_G(\delta_S^*)}_{\text{within-subspace metric error}}, \end{aligned}$$

where $\delta_S^ = \arg \min\{\delta^\top G \delta : q^\top \delta = \rho, \delta \in V_S\}$ is the Fisher-optimal direction restricted to the selected heads.*

Proof. This is a direct application of the Fisher-Pythagorean identity (Theorem G.1) twice: first decomposing δ_G^* vs. δ_S^* (the cost of restricting to a subspace), then δ_S^* vs. δ_{ITI} (the cost of using I instead of $G|_{V_S}$ within the subspace). The cross-terms vanish by the same orthogonality argument. \square

H Layer-wise Recursive Structure: Extended Proofs

H.1 Recursive Decomposition (Theorem 3.3)

Proof. The composite Jacobian factors as $J_{\ell \rightarrow L} = J_{\ell+1 \rightarrow L} A_\ell$, where $A_\ell = \partial h^{(\ell+1)} / \partial h^{(\ell)}$. Then:

$$\begin{aligned} G^{(\ell)} &= J_{\ell \rightarrow L}^\top G^{(L)} J_{\ell \rightarrow L} \\ &= (J_{\ell+1 \rightarrow L} A_\ell)^\top G^{(L)} (J_{\ell+1 \rightarrow L} A_\ell) \\ &= A_\ell^\top \underbrace{J_{\ell+1 \rightarrow L}^\top G^{(L)} J_{\ell+1 \rightarrow L}}_{G^{(\ell+1)}} A_\ell. \quad \square \end{aligned}$$

H.2 Condition Number Depth Bound (Theorem 3.4)

Proof. By the recursive decomposition:

$$\kappa(G^{(\ell)}) \leq \kappa(G^{(\ell+1)}) \cdot \kappa(A_\ell)^2.$$

For $A_k = I + B_k$ with $\|B_k\|_2 \leq \rho_k < 1$:

$$\sigma_{\max}(A_k) \leq 1 + \rho_k,$$

$$\sigma_{\min}(A_k) \geq 1 - \rho_k,$$

so $\kappa(A_k) \leq (1 + \rho_k)/(1 - \rho_k)$. Applying inductively from layer $L - 1$ down to layer ℓ :

$$\kappa(G^{(\ell)}) \leq \kappa(G^{(L)}) \prod_{k=\ell}^{L-1} \left(\frac{1 + \rho_k}{1 - \rho_k} \right)^2. \quad \square$$

H.3 Effective Rank Decay (Corollary 3.5)

Proof. From $G^{(\ell)} = A_\ell^\top G^{(\ell+1)} A_\ell$:

$$\text{tr}(G^{(\ell)}) = \text{tr}(A_\ell^\top G^{(\ell+1)} A_\ell) \geq \sigma_{\min}(A_\ell)^2 \text{tr}(G^{(\ell+1)}),$$

$$\lambda_{\max}(G^{(\ell)}) \leq \sigma_{\max}(A_\ell)^2 \lambda_{\max}(G^{(\ell+1)}).$$

Taking the ratio:

$$r_{\text{tr}}(G^{(\ell)}) = \frac{\text{tr}(G^{(\ell)})}{\lambda_{\max}(G^{(\ell)})} \geq \frac{r_{\text{tr}}(G^{(\ell+1)})}{\kappa(A_\ell)^2}. \quad \square$$

H.4 Euclidean Deviation Identity (Proposition 3.6)

Proof. The best scalar c^* minimizes $\|G - cI\|_F^2 = \text{tr}(G^2) - 2c \text{tr}(G) + c^2 d$, giving $c^* = \text{tr}(G)/d$. Then:

$$\begin{aligned} \|G - c^* I\|_F^2 &= \text{tr}(G^2) - \frac{(\text{tr} G)^2}{d} \\ &= \|G\|_F^2 \left(1 - \frac{\text{PR}(G)}{d} \right), \end{aligned}$$

where $\text{PR}(G) = (\text{tr} G)^2 / \text{tr}(G^2)$. Taking the square root and dividing by $\|G\|_F$ gives the result. \square

I Natural Gradient Equivalence

Theorem I.1 (Fisher steering as natural gradient). *Consider the per-sample cross-entropy loss $\mathcal{L}(h) = -\log P_{f(h)}(y)$ for an observed token y . The natural gradient step on h with Fisher information $G^{(\ell)} = J^\top H J$ is*

$$\delta h_{\text{NG}} = -\eta G^{-1} \nabla_h \mathcal{L} = -\eta G^{-1} J^\top (\phi - \gamma_y),$$

where $\phi = \nabla A(\lambda)$ and γ_y is the unembedding vector for token y . This is the Fisher-optimal direction for the covector $q = -\nabla_h \mathcal{L} = J^\top (\gamma_y - \phi)$.

Proof. The gradient is $\nabla_h \mathcal{L} = J^\top \nabla_\lambda \mathcal{L} = J^\top (\phi - \gamma_y)$. The natural gradient preconditions by G^{-1} :

$$\delta h_{\text{NG}} = -\eta (J^\top H J)^{-1} J^\top (\phi - \gamma_y).$$

This has the same form as our steering equation $(G + \alpha I)^{-1} q$ with $\alpha = 0$ and covector $q = J^\top (\gamma_y - \phi)$. \square

For a restricted subspace $h \in h_0 + \text{Im}(B)$ with $B \in \mathbb{R}^{d \times r}$ ($r \ll d$), the projected natural gradient is

$$\delta h = B (B^\top G B)^{-1} B^\top q,$$

which recovers the K-FAC / low-rank natural gradient form. Full-rank Fisher steering corresponds to $B = I$.

J LayerNorm Kernel Analysis

Proposition J.1 (LayerNorm Jacobian structure). *For a pre-LN residual block $h^{(\ell+1)} = h^{(\ell)} + F(\text{LN}(h^{(\ell)}))$, the block Jacobian is*

$$A_\ell = I + DF_\ell \cdot J_{\text{LN}},$$

where $J_{\text{LN}} = \partial \text{LN}(h) / \partial h$. The LayerNorm Jacobian satisfies

$$J_{\text{LN}} h = 0,$$

i.e., h itself lies in the kernel of J_{LN} . Consequently, $A_\ell h = h$ and the current hidden state is a fixed point of the block Jacobian.

Proof. LayerNorm computes $\text{LN}(h) = \gamma \odot (h - \mu \mathbf{1}) / \sigma + \beta$, where $\mu = \mathbf{1}^\top h / d$ and $\sigma = \|(h - \mu \mathbf{1})\| / \sqrt{d}$. Its Jacobian is

$$J_{\text{LN}} = \frac{\gamma}{\sigma} \odot \left(I - \frac{\mathbf{1}\mathbf{1}^\top}{d} - \frac{\bar{h}\bar{h}^\top}{\|\bar{h}\|^2} \right),$$

where $\bar{h} = h - \mu \mathbf{1}$. Applying to h :

$$\begin{aligned} \left(I - \frac{\mathbf{1}\mathbf{1}^\top}{d} \right) h &= h - \mu \mathbf{1} = \bar{h}, \\ \frac{\bar{h}\bar{h}^\top}{\|\bar{h}\|^2} h &= \frac{\bar{h} (\bar{h}^\top h)}{\|\bar{h}\|^2} = \frac{\bar{h} \|\bar{h}\|^2}{\|\bar{h}\|^2} = \bar{h}. \end{aligned}$$

Therefore $J_{\text{LN}} h = (\gamma/\sigma) \odot (\bar{h} - \bar{h}) = 0$.

For the block Jacobian: $A_\ell h = h + DF_\ell J_{\text{LN}} h = h + 0 = h$. \square

This result implies that the residual connection preserves the current hidden state as a fixed point of each block's linearization. Perturbations along h itself are invisible to the LayerNorm and therefore have zero Fisher cost, contributing to the large null space of $G^{(\ell)}$ observed in Experiment 2.